Diagonal-norm upwind SBP operators

Ken Mattsson *

June 8, 2016

Abstract

High-order accurate first derivative finite difference operators are derived that naturally introduce artificial dissipation. The boundary closures are based on the diagonal-norm summation-by-parts (SBP) framework and the boundary conditions are imposed using a penalty (SAT) technique, to guarantee linear stability for a large class of initial boundary value problems. These novel first derivative SBP operators have a non-central difference stencil in the interior, and come in pairs (for each order of accuracy). The resulting SBP-SAT approximations lead to fully explicit ODE systems. The accuracy and stability properties are demonstrated for linear first- and second-order hyperbolic problems in 1D, and for the compressible Euler equations in 2D. The newly derived first derivative SBP operators lead to significantly more robust and accurate numerical approximations, compared with the usage of (previously derived) central difference first derivative SBP operators.

Key words: finite difference methods, artificial dissipation, high-order accuracy, stability, boundary treatment

1 Introduction

It is well known that higher order methods (as compared to first- and second-order accurate methods) capture wave dominated phenomena more efficiently since they allow a considerable reduction in the degrees of freedom, for a given error tolerance. In particular, high-order finite difference methods

*Department of Information Technology, Uppsala University, P O Box 337, S-751 05 Uppsala, Sweden. telephone: +46-18-4717631, telefax: +46-18-523049, E–mail: ken.mattsson@it.uu.se

(HOFDMs) are ideally suited for problems of this type. (See the pioneering paper by Kreiss and Oliger [13] concerning hyperbolic problems.) The major difficulty with HOFDM is to obtain a stable boundary treatment, something that has received considerable past attention concerning hyperbolic and parabolic problems. (For examples, see [14, 32, 30, 1, 3, 10].) Roughly speaking, the numerical difficulties increase with the order of the spatial (and temporal) derivatives. For wave-dominated problems, in particular, it is imperative to use finite difference approximations that do not allow growth in time—a property termed "strict stability" [9].

A robust and well-proven high-order finite difference methodology, for well-posed initial boundary value problems (IBVP), is to combine summation-by-parts (SBP) operators [12, 31, 18] and either the simultaneous approximation term (SAT) method [4], or the projection method [27, 28, 19, 29] to impose boundary conditions (BC). Recent examples of the SBP-SAT approach can be found in [11, 16, 2, 25, 8, 24].

The SBP operators found in literature (see for example [12, 31, 18, 22, 23, 5]) are essentially central finite difference stencils closed at the boundaries with a careful choice of one-sided difference stencils, to mimic the underlying integration-by-parts formula in a discrete norm. SBP operators for various derivative orders can be constructed by repeated application of a central-difference first derivative SBP operator, here denoted D_1. For example, $D_1 D_1$ is a second derivative SBP operator, and is denoted a *wide stencil* second derivative SBP operator in the present study. For linear IBVP with smooth data (here referring either to physical data or the underlying curvilinear grid) an SBP-SAT approximation constructed from D_1 operators yields a strictly stable and accurate approximation. For IBVP with non-smooth data (or nonlinear problems), the exclusive usage of D_1 operators in combination with SAT (or projection) does not guarantee strict stability. For nonlinear first order hyperbolic or hyperbolic-parabolic IBVP (such as the Navier-Stokes equation) the addition of artificial dissipation (AD) is most often necessary, to damp spurious oscillations. Adding robust and accurate AD is however far from trivial, and most often involves tuning of "free" parameters. It is imperative that the addition of AD does not destroy the linear stability and accuracy properties, which in practice requires a very careful boundary closure of the added AD. How to add AD to traditional (central difference) SBP-SAT approximations based on D_1 was analysed in [20].

For second order hyperbolic IBVP a well-known cure to supress spurious oscillations (when non-smooth features are present) is to employ compatible narrow-stencil second derivative SBP operators (see for example [21, 22]), instead of using a wide-stencil approximation based on D_1. The narrow-stencil second derivative SBP operators are very accurate, but perhaps less

straightforward to implement in large-scale 2D or 3D problems involving mixed variable coefficient second derivative terms (see for example [38, 7]).

The main motivation in [6] for introducing *dual-pair* SBP operators was to introduce damping of spurious oscillations when discretising second order hyperbolic equations. The *dual-pair* SBP operators are first derivative operators with non-central finite difference stencils in the interior. In [6] up to $8th$ order accurate dual-pair SBP operators are mentioned, but only the $4th$ order accurate case is presented explicitly. To obtain stability the dual-pair SBP operators are combined with the projection method in [6]. In the present study, dual-pair SBP operators with an additional stability constraint are derived, and further combined with the SAT method for imposing BC. These novel SBP operators are here referred to as *upwind* SBP operators since they naturally introduce AD when combined with flux-splitting techniques for hyperbolic systems. (The dual-pair SBP operators in [6] do not have this property.) The novel upwind SBP operators lead to highly robust and accurate discretisations of hyperbolic problems, corroborated through numerical computations of both linear and nonlinear problems. The usefulness for hyperbolic-parabolic systems such as the Navier-Stokes equations, is indicated through stability proofs.

In Section 2 the novel upwind SBP definition is presented, including details of the necessary steps in the derivation. In Section 3 the SBP-SAT method is introduced for linear first- and second-order hyperbolic problems in 1D. In Section 4 the accuracy and stability properties of the newly developed upwind SBP operators are verified and compared to previously derived central difference SBP operators, by performing numerical simulations. The stability analysis is extended to 2D hyperbolic-parabolic systems in Section 5. Verification of accuracy and stability by numerical long-time simulations of an analytic 2D Euler vortex on a multiblock grid is presented in Section 6. Section 7 summarizes the work. The upwind SBP operators are presented in the Appendix.

2 The finite difference method

Previously derived SBP operators (see for example[12, 31, 18, 22, 16, 15, 23, 5]) are essentially central finite difference stencils closed at the boundaries with a careful choice of one-sided difference stencils, to mimic the underlying integration-by-parts formula in a discrete norm. In the present paper the SBP operators are addressed by the accuracy of the interior finite difference stencil. Finite difference SBP operators may be further categorised by the structure of their norm: a) diagonal, b) diagonal interior with block boundary

closures, c) fully banded. In the present study the focus is on the derivation of a novel type of diagonal-norm first derivative SBP operator, with a non-central interior stencil. The motivation is to naturally (,i.e., without tuning of "free" parameters) introduce AD without ruining linear stability.

2.1 Definitions

The following definitions are needed later in the present study. Let $\mathbf{u}, \mathbf{v} \in L^2[x_l, x_r]$ where $\mathbf{u}^T = [u^{(1)}, \ , u^{(2)}, \ldots, u^{(k)}]$ and $\mathbf{v}^T = [v^{(1)}, \ , v^{(2)}, \ldots, v^{(k)}]$ are real-valued vector functions with k components. Let the inner product be defined by $(\mathbf{u}, \mathbf{v})_{\mathbf{A}} = \int_{x_l}^{x_r} \mathbf{u}^T \mathbf{A}(x)\, \mathbf{v}\, dx$, $\mathbf{A}(x) = \mathbf{A}^T(x) > 0$, and let the corresponding norm be $\|\mathbf{u}\|_{\mathbf{A}}^2 = (\mathbf{u}, \mathbf{u})$.

The domain ($x_l \leq x \leq x_r$) is discretized using the following m equidistant grid points:

$$x_i = x_l + (i-1)\, h, \quad i = 1, 2, \ldots, m, \quad h = \tfrac{x_r - x_l}{m-1} \ .$$

The following vectors will be used frequently:

$$\begin{aligned} &\mathbf{x} = [x_1,\, x_2, \ldots, x_{m-1},\, x_m]^T, \quad \mathbf{x}^q = \tfrac{1}{q!}[x_1^q,\, x_2^q, \ldots, x_{m-1}^q,\, x_m^q]^T \\ &\mathbf{1} = \mathbf{x}^0 = [1,\, 1, \ldots, 1,\, 1]^T, \qquad \mathbf{0} = [0,\, 0, \ldots, 0,\, 0]^T \\ &e_1 = [1, 0, \ldots, 0]^T, \qquad\qquad e_m = [0, \ldots, 0, 1]^T \ , \\ &B = e_m e_m^T - e_1 e_1^T \ . \end{aligned} \tag{1}$$

The following definition is important for the stability analysis,

Definition 2.1 *Let $L = x_r - x_l$ denote the width of the domain, and $h = \frac{L}{m-1}$ the grid-spacing. A symmetric positive definite matrix H defines a discrete norm if $\mathbf{1}^T H \mathbf{1} = L$, independent of the number of grid-points m.*

The analysis in the present study will utilise the Kronecker product,

$$C \otimes D = \begin{bmatrix} c_{0,0}\, D & \cdots & c_{0,q-1}\, D \\ \vdots & & \vdots \\ c_{p-1,0}\, D & \cdots & c_{p-1,q-1}\, D \end{bmatrix} \ ,$$

where C is a $p \times q$ matrix and D is an $m \times n$ matrix. Two useful rules for the Kronecker product are $(A \otimes B)(C \otimes D) = (AC) \otimes (BD)$ and $(A \otimes B)^T = A^T \otimes B^T$.

The approximate solution vector is given by $v^T = [v^{(1)}, v^{(2)}, \ldots, v^{(k)}]$, where $v^{(j)} = [v_1^{(j)}, v_2^{(j)}, \ldots, v_m^{(j)}]$ is the discrete solution vector of the jth component. Let I_k denote the unit matrix of size $k \times k$ and A the projection of $\mathbf{A}(x)$ onto the block diagonals. $\tilde{H} = I_k \otimes H$ defines a discrete norm, since H defines a discrete norm. An inner product for discrete real-valued vector functions $u, v \in \mathbf{R^{k \times m}}$ is defined by $(u, v)_{HA} = u^T A\tilde{H} v$. The corresponding norm is $\|v\|_{HA}^2 = v^T \tilde{H} A v$.

Remark The matrix product $\tilde{H}A$ defines a norm if and only if $\tilde{H}A$ is symmetric and positive definite and $\tilde{H}$ defines a discrete norm. For variable $A(x)$ this can only be guaranteed if the discrete norm H is a diagonal matrix (see [33] for a detailed study on this). Variable coefficients are often present due to the underlying physics or the geometry requiring the introduction of curvilinear grids.

The following 3 definitions are central to the present study:

Definition 2.2 *An explicit pth-order accurate finite difference scheme with minimal stencil width for the Cauchy problem is denoted a pth-order accurate narrow-stencil.*

Definition 2.3 *A difference operator* $D_1 = H^{-1}\left(Q + \frac{B}{2}\right)$ *approximating* $\partial/\partial x$*, using a pth-order accurate interior stencil, is said to be a pth-order diagonal-norm first-derivative SBP operator if the diagonal matrix* H *defines a discrete norm, and* $Q + Q^T = 0$*.*

Definition 2.4 *A difference operator* $D_2^{(a)} = H^{-1}(-M^{(a)} + a_m e_m d_{1;m} - a_1 e_1 d_{1;1})$ *approximating* $\partial/\partial x\,(a\,\partial/\partial x)$*, where* $a > 0$*, using a pth-order accurate stencil in the interior, is said to be a pth-order diagonal-norm second-derivative SBP operator if the diagonal matrix* H *defines a discrete norm,* $M^{(a)} = (M^{(a)})^T \geq 0$*,* $d_{1;1}v \simeq u_x|^0$ *and* $d_{1;m}v \simeq u_x|^L$ *are finite difference approximations of the first derivative at the left and right boundary points.*

The matrix B and the vectors e_1 and e_m are defined in (1). In the present study, narrow-stencil SBP operators will be referred to as *traditional* SBP operators. Traditional first derivative SBP operators were first derived in [12, 31], and later improved in [16, 15]. Similarly, traditional second derivative SBP operators were derived in [22]. (Recently, high-order accurate traditional SBP operators for third and fourth derivatives were derived [23].) For the constant coefficient case, $D_2^{(a)} = a\,D_2$ where D_2 is an approximation of $\partial^2/\partial x^2$. High-order accurate traditional D_2 operators were derived in [18]. The following lemma (first introduced in [17]) is central to the present study:

second-order	fourth-order	sixth-order
1	0.2508560249	0.1878715026

Table 1: α_1 in Eq. 2 for the diagonal-norm second-, fourth- and sixth-order accurate diagonal-norm second-derivative SBP operators.

Lemma 2.5 *The dissipative part $M^{(a)}$ of a second-derivative SBP operator has the following property:*

$$v^T M^{(a)} v = h\,\frac{\alpha_1}{a_1}(d_{1;1}v)^2 + h\,\frac{\alpha_1}{a_m}(d_{1;m}v)^2 + v^T \tilde{M^{(a)}} v\ , \tag{2}$$

where $\tilde{M^{(a)}}$ is symmetric and positive semi-definite, and α_1 a positive constant, independent of h.

For the special but important case of constant coefficients ($a = 1$) the numerically derived values of α_1 for the traditional diagonal-norm second-, fourth- and sixth-order accurate D_2 operators are presented in Table 1. (For the analysis of the variable coefficient case, see [38].)

Remark For a wide-stencil diagonal-norm second derivative SBP operator $D_2^{(a)}$, it is trivial to show that $\alpha_1 = h_{1,\,1}$ and $\alpha_m = h_{m,\,m}$ in Lemma 2.5 , where $h_{1,\,1}$ and $h_{m,\,m}$ are the first and last elements in the norm matrix H.

2.2 Upwind SBP operators

In a recent paper [6] a modified first derivative SBP definition is introduced. The SBP operators presented in [6] are here referred to as *dual-pair SBP operators*, and are employing non-central interior stencils. For completeness the general definition of dual-pair SBP operators is restated below:

Definition 2.6 *The difference operators $D_+ = H^{-1}\left(Q_+ + \frac{B}{2}\right)$ and $D_- = H^{-1}\left(Q_- + \frac{B}{2}\right)$ approximating $\partial/\partial x$, using pth-order accurate interior stencils, are said to be pth-order diagonal-norm dual-pair SBP operators if the diagonal matrix H defines a discrete norm, and $Q_+ + Q_-^T = 0$.*

The interior difference stencil of the *dual-pair SBP operators* derived in [6] were skewed by two grid-cells, as compared to a central stencil. The Definition 2.6 is more general as it could encompass more or less skewness (for example one or three grid-cells, instead of two). The motivation in [6] for introducing dual-pair SBP operators was to introduce damping of spurious oscillations when discretising second order hyperbolic equations. It is well-known that odd order finite difference schemes using a central finite difference

stencil (for example in traditional first derivative SBP operators) do not damp spurious oscillations, that are typically triggered by unresolved features in the solution or by non-smooth coefficients.

In the present study, a subclass of diagonal-norm dual-pair SBP operators is introduced, here referred to as *upwind SBP operators*, with an additional stability constraint necessary when applied to first order hyperbolic systems and hyperbolic-parabolic systems (such as the Navier-Stokes equations). The following new definition is one of the main results of the present study:

Definition 2.7 *The difference operators* $D_+ = H^{-1}\left(Q_+ + \frac{B}{2}\right)$ *and* $D_- = H^{-1}\left(Q_- + \frac{B}{2}\right)$ *approximating* $\partial/\partial x$*, using pth-order accurate interior stencils, are said to be pth-order diagonal-norm upwind SBP operators if the diagonal matrix* H *defines a discrete norm,* $Q_+ + Q_-^T = 0$*, and* $Q_+ + Q_+^T = \frac{S}{2}$ *is negative semi-definite.*

Hence, *upwind SBP operators* are *dual-pair SBP operators* with the additional requirement that $Q_+ + Q_+^T = \frac{S}{2}$ is negative semi-definite. This additional constraint will naturally introduce artificial dissipation when combining upwind SBP operators and flux-splitting techniques, when discretising first order hyperbolic (or hyperbolic-parabolic) systems. (The dual-pair SBP operators in [6] do not have this property.) In the present study, *upwind SBP operators* of both odd- and even-orders will be derived, up to $9th$ order. (For the odd order cases, the interior stencil is skewed by one grid-cell, while the even order cases are skewed by two grid-cells such as in [6].)

A few useful relations involving diagonal-norm first derivative upwind SBP operators are given,

$$\begin{aligned}
&\tfrac{D_+ + D_-}{2} = H^{-1}\left(\tfrac{Q_+ + Q_-}{2} + \tfrac{B}{2}\right) = H^{-1}\left(Q + \tfrac{B}{2}\right) = D_1 \,, \\
&\tfrac{D_+ - D_-}{2} = H^{-1}\left(\tfrac{Q_+ - Q_-}{2}\right) = H^{-1}\left(\tfrac{Q_+ + Q_+^T}{2}\right) = H^{-1}S \,, \\
&HD_- = -(D_+)^T H + B, \quad HD_+ = -(D_-)^T H + B \,,
\end{aligned} \tag{3}$$

where $Q = -Q^T$ and $S = S^T \leq 0$. Hence $\frac{D_+ + D_-}{2}$ is a first derivative SBP operator with a central finite difference scheme in the interior, and $\frac{D_+ - D_-}{2}$ is a negative definite finite difference operator (that will act as an artificial dissipation operator).

Let the diagonal matrix A be the projection of some smooth function $a > 0$ onto the diagonal. The following relations are useful in the coming

stability analysis,

$$
\begin{aligned}
D_{2-}^{(a)} &= D_+ A D_- = H^{-1}(-D_-^T H A D_- + B A D_-) \,, \\
D_{2+}^{(a)} &= D_- A D_+ = H^{-1}(-D_+^T H A D_+ + B A D_+) \,, \\
D_{2+-}^{(a)} &= \tfrac{D_{2-}^{(a)} + D_{2+}^{(a)}}{2} = H^{-1}(-\tfrac{D_-^T H A D_- + D_+^T H A D_+}{2} + B A \tfrac{D_+ + D_-}{2}) \,.
\end{aligned}
\tag{4}
$$

Hence, $D_{2-}^{(a)}$, $D_{2-}^{(a)}$ and $D_{2+-}^{(a)}$ are all diagonal-norm second-derivative SBP operators according to Definition 2.4.

The following new definition is one of the main results of the present study:

Definition 2.8 *Let the diagonal matrix A be the projection of some smooth function $a > 0$ onto the diagonal. The difference operators $D_{2-}^{(a)} = D_+ A D_-$ and $D_{2+}^{(a)} = D_- A D_+$ approximating $\partial/\partial\, x\,(\, a\, \partial/\partial\, x)$, where D_+ and D_- are pth-order diagonal-norm upwind SBP operators, are said to be pth-order diagonal-norm second-derivative upwind SBP operators.*

In the present study the focus is on diagonal-norm SBP operators, and from now on *diagonal norm* will be omitted when referring to the various SBP operators.

To elucidate the difference between traditional SBP operators and upwind SBP operators consider the following problem,

$$
\theta u_t = a u_x + (\gamma u_x)_x, \quad x_l \le x \le x_r, \quad t \ge 0 \,,
\tag{5}
$$

where $a > 0$ is a constant coefficient, and $\theta > 0$, $\gamma > 0$ are time-independent parameters (that can depend on x). (Here also assuming initial data $u(x,0) = f(x)$.) Multiplying (5) by u, integrating by parts (IBP) and adding the transpose leads to,

$$
\frac{d}{dt}\|u\|_\theta^2 = BT + DI \,,
\tag{6}
$$

where the boundary terms (BT) and the dissipation (DI) are given by,

$$
\begin{aligned}
BT &= (a u^2 + 2 u \gamma u_x)|^{x_r} - (a u^2 + 2 u \gamma u_x)|^{x_l} \,, \\
DI &= -2\, \|u_x\|_\gamma^2 \,.
\end{aligned}
\tag{7}
$$

The semi-discrete approximation of (5) using a traditional first derivative SBP operator D_1 is given by,

$$
\Theta v_t = a D_1 v + D_1 \Gamma D_1 v, \quad t \ge 0 \,,
\tag{8}
$$

where the diagonal matrices Θ and Γ are the projections of θ and γ onto the diagonals, respectively. Multiply (8) by $v^T H$ and add the transpose to obtain,

$$\frac{d}{dt}\|v\|^2_{H\Theta} = BT_h + DI_h \ , \tag{9}$$

where the semi-discrete boundary terms (BT_h) and the dissipation (DI_h) are given by,

$$\begin{aligned} BT_h &= (av_m^2 + 2v_m\gamma_m(D_1 v)_m) - (av_1^2 + 2v_1\gamma_1(D_1 v)_1) \ , \\ DI_h &= 2\,(D_1 v)^T H\Gamma(D_1 v) \ . \end{aligned} \tag{10}$$

Eq. 9 exactly mimics Eq. 6, except for the highest frequency mode, often referred to as the π-mode. It is well-known that the π-mode is unaltered by centered difference approximations of odd orders, (see for example [20, 22]). The interior stencil of traditional first derivative SBP operators are central difference approximations. For nonlinear problems (here assuming $a = a(u)$) or problems with non-smooth coefficients, some type of AD is required to damp the π-mode. The semi-discrete approximation of (5), now using the upwind SBP operators D_+ and D_- is given by,

$$\Theta v_t = aD_+ v + D_+ \Gamma D_- v, \quad t \geq 0 \ , \tag{11}$$

where $a > 0$. (The case where $a < 0$ would instead have $aD_- v$, for the convective term.) Multiply (11) by $v^T H$ and add the transpose to obtain,

$$\frac{d}{dt}\|v\|^2_{H\Theta} = BT_{h-} + DI_{h-} + AD_h \ , \tag{12}$$

where the semi-discrete artificial damping (AD_h), the boundary terms (BT_{h-}) and the dissipation (DI_{h-}) are given by,

$$\begin{aligned} BT_{h-} &= (av_m^2 + 2v_m\gamma_m(D_- v)_m) - (av_1^2 + 2v_1\gamma_1(D_- v)_1) \ , \\ DI_{h-} &= 2\,(D_- v)^T H\Gamma(D_- v) \ , \\ AD_h &= a\, v^T(Q_+ + Q_+^T)v \ . \end{aligned} \tag{13}$$

Eq. 12 exactly mimics Eq. 6, even in the presens of the π-mode, since the interior stencil of D_- is a non-central difference stencil. The additional AD_h term introduces efficient damping even when γ (that governs the physical dissipation or diffusion of the problem) is small (or zero). To summarise: the major difference between employing traditional and upwind SBP operators is that upwind SBP operators introduce AD. Both types of SBP operators mimic the IBP property.

2.3 Construction of SBP operators

For the reader interested in the construction of the upwind SBP operators, the procedure will be outlined in some detail. First some definitions are needed, before motivating the necessary order of steps. Let $\tilde{D} = H^{-1}(\tilde{Q} + \frac{B}{2})$ denote either a traditional SBP operator (i.e., D_1, given by Definition 2.3) or an upwind SBP operator (i.e., $D_\pm$, given by Definition 2.7). The following two new definitions are central to the present study.

Definition 2.9 *Let* $\mathbf{x}^q$ *be the projection of the polynomial* $\frac{x^q}{q!}$ *onto the discrete grid-points, i.e., a vector denoted* $\mathbf{x}$*. Let* $e_{(q)} = H\mathbf{x}^{q-1} - \left(\tilde{Q} + \frac{B}{2}\right)\mathbf{x}^q$ *be the* q*th order error vector. We say that* $\tilde{D}$ *is* p*th-order if* $e_{(q)}$ *vanishes for* $q = 1 \dots p$*, in the interior and for* $q = 1 \dots s/2$*, at the boundaries where* $s = p$ *when* p *is even and* $s = p - 1$ *when* p *is odd.*

Definition 2.10 *Let* $\mathbf{x}^q$ *be the projection of the polynomial* $\frac{x^q}{q!}$ *onto the discrete grid-points, i.e., a vector denoted* $\mathbf{x}$*. Let* $e_{(q)} = H\mathbf{x}^{q-1} - \left(\tilde{Q} + \frac{B}{2}\right)\mathbf{x}^q$ *be the* q*th order error vector. The discrete* l_2*-norm of the error* $e_{(q)}$ *is defined as* $\|e_{(q)}\|_h^2 = h\, e_{(q)}^T e_{(q)}$*.*

It is important to understand that the formal boundary accuracy alone does not dictate the expected convergence rate of the numerical approximation. The expected convergence rate can be shown by a careful error analysis (not presented in the present study). This is summarised in the following remark:

Remark In [37] it is shown that a pointwise stable approximation of an IBVP involving derivatives up to order q yields a convergence rate of order $q + r$, where r is the order of accuracy at the boundaries. Let p denote the internal accuracy of a diagonal-norm SBP operator (both traditional and upwind). For the cases when p is even the boundary closure is restricted to $p/2th$-order accuracy (see [18]), i.e., $e_{(p/2+1)}$ is the leading order error. For the odd orders cases the leading order error is given by $e_{((p-1)/2+1)}$. This implies that the convergence rate drops to $(r+1)th$ order for first order hyperbolic problems, and $(r+2)th$ order for parabolic problems and second order hyperbolic problems, where r denotes the boundary accuracy. As an example, the $8th$ and $9th$ order upwind SBP operators have $r = 4$. In the present study pointwise stability is not proven, but the numerical convergence studies presented in Sections 4 and 6 indicate that the expected convergence rates (from the assumption of pointwise stability) are obtained.

Let p denote the interior accuracy. The construction of even-order diagonal-norm upwind (or traditional) SBP operators (up to $8th$ order) require at least p boundary points with $p/2th$ order accurate boundary stencils. Similarly, the odd-order (upwind) cases (up to $9th$ order), require at least $p-1$ boundary points with $(p-1)/2th$ order accurate boundary stencils.

2.3.1 Procedure

The first step when building SBP operators is to make sure that the symmetry requirements for the various matrices involved are met, and at the same time include sufficiently many unknowns in the boundary closures to fulfill the accuracy requirements. The SBP operators are derived using Maple, a symbolic math software (although any software with symbolic math tools can be used).

The interior stencil of the upwind SBP operator D_+ of order p (and $p+1$) starts from the central narrow-stencil of order $p+2$. Then subtract $\frac{h^{p+1}}{\alpha_p}(\Delta_+\Delta_-)^{p/2+1}$ to get rid of the outer grid-point to the left. Here $\Delta_\pm$ are the standard forward and backward finite difference operators and the parameter α_p varies with the order of accuracy. This yields a $p+1$ order accurate skewed stencil, and represents the interior stencil of the $(p+1)th$ order upwind SBP operator D_+. To obtain the interior stencil of the pth order upwind SBP operator D_+, continue to subtract $\frac{h^p}{\beta_p}\Delta_-(\Delta_+\Delta_-)^{p/2-2}$ to get rid of the next outer most term to the left. Hence, the scheme will now be off-centered by two grid-points.

The structure of Q_+ is given by the Ansatz:

$$
\begin{bmatrix}
q_{1,1} & q_{1,2} & \cdots & q_{1,\tilde{s}} & & & & & & & & \\
q_{2,1} & \ddots & & q_{2,\tilde{s}} & & & & & & & & \\
\vdots & & & \vdots & q_{\frac{s}{2}+1} & & & & & & & \\
\vdots & & & \vdots & \vdots & & & & & & & \\
q_{\tilde{s},1} & q_{\tilde{s},2} & \cdots & q_{\tilde{s},\tilde{s}} & q_1 & \ddots & \ddots & & & & & \\
 & & q_{n-\frac{s}{2}} & \cdots & q_0 & q_1 & \cdots & q_{\frac{s}{2}+1} & & & & \\
 & & & \ddots & & \ddots & & & \ddots & & & \\
 & & & & q_{n-\frac{s}{2}} & \cdots & q_0 & q_1 & \cdots & q_{\frac{s}{2}+1} & & \\
 & & & & & \ddots & & \ddots & q_{\tilde{s},\tilde{s}} & q_{\tilde{s}-1,s} & \cdots & q_{1,\tilde{s}} \\
 & & & & & & \ddots & & q_{\tilde{s},\tilde{s}-1} & \ddots & & q_{1,\tilde{s}-1} \\
 & & & & & & & q_{n-\frac{s}{2}} & \vdots & & & \vdots \\
 & & & & & & & & \vdots & & & \vdots \\
 & & & & & & & & q_{\tilde{s},1} & \cdots & & q_{1,1}
\end{bmatrix}
$$

Let p denote the internal order of accuracy. In the present study, upwind SBP operators of orders $p = 2, 4, 6, 8$ (even order cases) and $p = 3, 5, 7, 9$ (odd order cases) are derived. For the odd order cases let $s = p - 1$ and $n = 2$ in the above matrix structure, and for the even order cases let $s = p$ and $n = 1$. To obtain $\frac{s}{2}th$-order accurate boundary closures in both D_+ and D_- at least s boundary points are needed, i.e., $\tilde{s} \geq s$ in the above Ansatz. In the present study operators with minimum number of boundary points are presented, i.e., $\tilde{s} = s$. The norm is given by the Ansatz $H = h \cdot diag(h_1, \ldots, h_s, 1 \ldots, 1, h_s, \ldots, h_1)$. Since Q_- is given by the relation $Q_- = -Q_+^T$, it is enough to present the coefficients in Q_+ and H, see Appendix.

The unknown in Q_+ and H are tuned to obey the accuracy requirements for both D_+ and D_-, presented in Definition 2.9. Here it is imperative that H be positive definite. There are "free" parameters left after imposing the accuracy and symmetry conditions, when $p > 3$. The $4th$ (and $5th$) order upwind case have 2 free parameters, the $6th$ (and $7th$) order have 4 free parameters and the $8th$ (and $9th$) have 9 free parameters.

Remark The traditional first derivative SBP operators have less "free" parameters to tune compared with the corresponding upwind SBP operators. The traditional $6th$ and $8th$ order cases have 1 and 3 free parameters, respectively.

When tuning these "free" parameters it is imperative to choose them such that the upwind SBP operators: 1) fulfil the extra requirement that $Q_+ + Q^T = \frac{S}{2}$ is negative semi-definite, and 2) have the most accurate boundary closures possible, by minimising the leading order error norm in Definition 2.10.

Remark For the 2nd and 3rd order upwind SBP operators, there are no free parameters if $\tilde{s} = s$ in the above ansatz. However, it is of course possible to extend the number of unknowns at the boundaries by allowing $\tilde{s} > s$, to obtain free parameters. The free parameters can then be tuned to obtain a possibly more accurate boundary closure, although the formal order of accuracy can not be improved [16]. A careful numerical study (not presented here) showed that the 2nd order upwind SBP operators with $\tilde{s} = 2$, compared to the corresponding SBP operators with $\tilde{s} = 3$ gave almost identical convergence results. Similarly, for the 3rd order case, upwind SBP operators with $\tilde{s} = 2$, $\tilde{s} = 3$ and $\tilde{s} = 4$ were derived. However, it turned out that they gave almost identical convergence results. Hence, only upwind SBP operators with $\tilde{s} = s$ are presented in the Appendix.

In the present study upwind SBP operators up to $9th$ order accuracy are derived, optimised for accuracy. The operators are presented in Appendix. Q_+ and H for the 3rd order case (when $m = 7$) are presented below,

$$Q_+ = \begin{bmatrix} -\frac{1}{12} & \frac{3}{4} & -\frac{1}{6} & 0 & 0 & 0 & 0 \\ -\frac{5}{12} & -\frac{5}{12} & 1 & -\frac{1}{6} & 0 & 0 & 0 \\ 0 & -\frac{1}{3} & -\frac{1}{2} & 1 & -\frac{1}{6} & 0 & 0 \\ 0 & 0 & -\frac{1}{3} & -\frac{1}{2} & 1 & -\frac{1}{6} & 0 \\ 0 & 0 & 0 & -\frac{1}{3} & -\frac{1}{2} & 1 & -\frac{1}{6} \\ 0 & 0 & 0 & 0 & -\frac{1}{3} & -\frac{5}{12} & \frac{3}{4} \\ 0 & 0 & 0 & 0 & 0 & -\frac{5}{12} & -\frac{1}{12} \end{bmatrix}, H = h \begin{bmatrix} \frac{5}{12} & 0 & 0 & 0 & 0 & 0 & 0 \\ 0 & \frac{13}{12} & 0 & 0 & 0 & 0 & 0 \\ 0 & 0 & 1 & 0 & 0 & 0 & 0 \\ 0 & 0 & 0 & 1 & 0 & 0 & 0 \\ 0 & 0 & 0 & 0 & 1 & 0 & 0 \\ 0 & 0 & 0 & 0 & 0 & \frac{13}{12} & 0 \\ 0 & 0 & 0 & 0 & 0 & 0 & \frac{5}{12} \end{bmatrix}.$$

3 Semi-discrete analysis in 1D

3.1 Flux-splitting

Consider

$$\mathbf{u}_t = \mathbf{A}\mathbf{u}_x, \quad x_l \leq x \leq x_r, \quad t \geq 0 \,, \tag{14}$$

where $\mathbf{A} = \mathbf{A}^T$ is a constant coefficient matrix of size $k \times k$. (Here also assuming initial data $\mathbf{u}(x, 0) = \mathbf{f}(x)$.) Multiplying Eq. 18 by $\mathbf{u}^T$, integrating by parts and adding the transpose leads to,

$$\frac{d}{dt}\|\mathbf{u}\|^2 = \mathbf{u}_r^T \mathbf{A}\mathbf{u}_r - \mathbf{u}_l^T \mathbf{A}\mathbf{u}_l \,. \tag{15}$$

Here $\mathbf{u}_{l,r}^T = [u_{l,r}^{(1)}, \ldots, u_{l,r}^{(k)}]$ are the unknowns at the left and right boundary, respectively.

Before proceeding to the semi-discrete approximation the convective term $\mathbf{Au}$ is split into two parts with positive and negative running characteristics, respectively (often referred to as flux splitting). The idea is to split $\mathbf{A}$ into a positive and a negative part, i.e. $\mathbf{A} = \mathbf{A}_+ + \mathbf{A}_-$. Here it is assumed that the eigenvalues of $\mathbf{A}_+$ are non-negative, and that the eigenvalues of $\mathbf{A}_-$ are non-positive. This can be done in a number of ways, but they all require diagonalizing $\mathbf{A}$, i.e., $\mathbf{A} = \mathbf{T}^\mathbf{T}\mathbf{\Lambda}\mathbf{T}$, where the diagonal matrix $\mathbf{\Lambda}$ holds the eigenvalues to $\mathbf{A}$. Define

$$2\,\mathbf{A}_\pm = \mathbf{T}^\mathbf{T}\left(\mathbf{\Lambda} \pm \mathbf{\Sigma}\right)\mathbf{T} = \mathbf{A} \pm \mathbf{R}\ ,$$

where $\mathbf{\Sigma}$ is a symmetric positive definite matrix such that $\mathbf{A}_+$ is positive (semi-) definite and $\mathbf{A}_-$ negative (semi-) definite. Note that $\mathbf{R}$ by construction is symmetric and positive (semi-) definite. Let α denote the absolute value of the largest (in magnitude) eigenvalue of $\mathbf{A}$ and let $|\mathbf{\Lambda}|$ denote a matrix with the absolute values of the eigenvalues on the diagonal.

A common flux-splitting is to use $\mathbf{\Sigma} = \alpha\mathbf{I_k}$, i.e.,

$$2\,\mathbf{A}_\pm = \mathbf{T}^\mathbf{T}\left(\mathbf{\Lambda} \pm \alpha\mathbf{I_k}\right)\mathbf{T} = \mathbf{A} \pm \alpha\mathbf{I_k}\ , \tag{16}$$

referred to as *Lax–Friedrich* flux-splitting. Here $R = \alpha\mathbf{I_k}$. Another choice is to use $\mathbf{\Sigma} = |\mathbf{\Lambda}|$, i.e.,

$$2\,\mathbf{A}_\pm = \mathbf{T}^\mathbf{T}\left(\mathbf{\Lambda} \pm |\mathbf{\Lambda}|\right)\mathbf{T} = \mathbf{A} \pm |\mathbf{A}|\ , \tag{17}$$

referred to as *Steger-Warming* flux splitting. Here $R = |\mathbf{A}|$. The hyperbolic system (14) can be written,

$$\mathbf{u}_t = \mathbf{A}_+\mathbf{u}_x + \mathbf{A}_-\mathbf{u}_x, \quad x_l \le x \le x_r, \quad t \ge 0\ , \tag{18}$$

utilizing the flux splitting.

A semi-discrete finite difference approximation of (18) using upwind SBP operators is given by

$$\begin{aligned} v_t &= \left(A_+ \otimes D_+\right)v + \left(A_- \otimes D_-\right)v \\ &= \left(A \otimes \frac{D_+ + D_-}{2}\right)v + \left(R \otimes \frac{D_+ - D_-}{2}\right)v \\ &= \left(A \otimes D_1\right)v + \left(R \otimes H^{-1}S\right)v\ . \end{aligned} \tag{19}$$

Hence, the combination of upwind SBP operators and flux splitting is equivalent to employing a central-difference first derivative SBP operator (see

Definition 2.3) to the non-split form (14), with the addition of artificial dissipation. Note that there are no "free" parameters to tune in the AD term $(R \otimes H^{-1}S)\, v$.

Multiplying Eq. 19 by $v^T I_k \otimes H$ and adding the transpose yields,

$$
\begin{aligned}
v^T(I_k \otimes H)v_t + v_t^T(I_k \otimes H)v &= v^T \left(A_+ \otimes (Q_+ + Q_+^T + B)\right) v \\
&+ v^T \left(A_- \otimes (Q_- + Q_-^T + B)\right) v \\
&= v^T \left(\frac{A}{2} \otimes (Q_+ + Q_+^T + Q_- + Q_-^T)\right) v \\
&+ v^T \left(\frac{R}{2} \otimes (Q_+ + Q_+^T - Q_- - Q_-^T)\right) v + v^T(A \otimes B)v \\
&= v^T \left(\frac{A}{2} \otimes (Q_+ + Q_+^T - Q_+^T - Q_+)\right) v \\
&+ v^T \left(\frac{R}{2} \otimes (Q_+ + Q_+^T + Q_+^T + Q_+)\right) v + v^T(A \otimes B)v \\
&= \left(R \otimes (Q_+ + Q_+^T)\right) v + v^T(A \otimes B)v \\
&\Downarrow \\
\frac{d}{dt}\|v\|_H^2 &= v^T \left(R \otimes S\right) v + v_r A v_r - v_l A v_l \,.
\end{aligned}
$$

Hence, the continuous energy estimate (22) is mimicked with the addition of artificial dissipation $v^T \left(R \otimes S\right) v$. $S = (Q_+ + Q_+^T)$ is negative semi-definite by construction (see Definition 2.7), and parameter free.

3.2 First order hyperbolic systems

How to achieve a stable finite difference approximations in 1-D, by combining the upwind SBP operators and the SAT method of imposing the physical BC is here presented. Consider the following hyperbolic system,

$$
\begin{array}{lll}
\mathbf{u}_t = \mathbf{A}\mathbf{u}_x & , \quad x_l \le x \le x_r, & t \ge 0 \\
\mathbf{u} = \mathbf{f} & , \quad x_l \le x \le x_r, & t = 0
\end{array} \quad , \tag{20}
$$

where

$$
\mathbf{A} = \begin{bmatrix} 0 & 1 \\ 1 & 0 \end{bmatrix} \,. \tag{21}
$$

Here performing *Steger-Warming* flux splitting,

$$
\mathbf{\Lambda} = \begin{bmatrix} -1 & 0 \\ 0 & 1 \end{bmatrix} \,, \quad |\mathbf{A}| = \begin{bmatrix} 1 & 0 \\ 0 & 1 \end{bmatrix} \,, \quad 2\,\mathbf{A}_+ = \begin{bmatrix} 1 & 1 \\ 1 & 1 \end{bmatrix} \,, \quad 2\,\mathbf{A}_- = \begin{bmatrix} -1 & 1 \\ 1 & -1 \end{bmatrix} \,.
$$

Multiplying the first equation in (20) by $\mathbf{u}^T$, integrating by parts and adding the transpose leads to,

$$\frac{d}{dt}\|\mathbf{u}\|^2 = \mathbf{u}_r^T \mathbf{A}\mathbf{u}_r - \mathbf{u}_l^T \mathbf{A}\mathbf{u}_l = 2u_r^{(1)}u_r^{(2)} - 2u_l^{(1)}u_l^{(2)} \ . \tag{22}$$

Here $\mathbf{u}_{l,\,r}^T = [u_{l,\,r}^{(1)} \quad u_{l,\,r}^{(2)}]$ are the unknowns at the left and right boundary, respectively. The eigenvalues of $\mathbf{A}$ are ± 1 and one boundary condition at each boundary should be specified . There are many possibilities but here the focus is on Dirichlet BC.

One set of well-posed BC is for example

$$\begin{array}{l} u_l^{(1)} = g_l(t) \\ u_r^{(1)} = g_r(t) \end{array} \ , \tag{23}$$

where $g_{l,\,r}(t)$ are the boundary data at the left and right boundary, respectively. The semi-discrete approximation of (23) is given by

$$\begin{array}{l} v_1^{(1)} = \left(e^{(1)} \otimes e_1^T\right) v = g_l(t) \\ v_m^{(1)} = \left(e^{(1)} \otimes e_m^T\right) v = g_r(t) \end{array} \ , \tag{24}$$

where $e^{(1)} = [1 \quad 0]$ and $e_{1,\,m}$ are given by (1).

The semi-discrete problem using the SBP-SAT method reads

$$\begin{aligned} v_t = (A_+ \otimes D_+)\, v + (A_- \otimes D_-)\, v + \tau_l \otimes H^{-1} e_1 \left(v_1^{(1)} - g_l(t)\right) \\ + \tau_r \otimes H^{-1} e_m \left(v_m^{(1)} - g_r(t)\right) \ , \end{aligned} \tag{25}$$

where $\tau_{l,\,r} = [\tau_{l,\,r}^{(1)},\ \tau_{l,\,r}^{(2)}]^T$ are the penalty vectors at the left and right boundary, respectively.

The following lemma is central to the present study.

Lemma 3.1 *The scheme (25) is stable if $D_\pm$ are upwind first derivative SBP operators, $\tau_l^{(2)} = 1$, $\tau_r^{(2)} = -1$, and $\tau_{l,\,r}^{(1)} \leq 0$ hold.*

Proof Multiplying the homogeneous version of (25) by $v^T I_2 \otimes H$ and adding

the transpose yields,

$$\begin{aligned} v^T(I_2 \otimes H)v_t + v_t^T(I_2 \otimes H)v &= v^T(A_+ \otimes (Q_+ + Q_+^T))v \\ &+ v^T(A_- \otimes (Q_- + Q_-^T))v = \\ &v^T(|A| \otimes S)v^T - v_1 A v_1 + v_m A v_m = \\ &v^T(|A| \otimes S)v^T - 2\tau_l^{(1)} v_1^{(1)} v_1^{(1)} - 2\tau_l^{(2)} v_1^{(1)} v_1^{(2)} \\ &- 2\tau_r^{(1)} v_m^{(1)} v_m^{(1)} - 2\tau_r^{(2)} v_m^{(1)} v_m^{(2)} \\ &\Downarrow \\ \frac{d}{dt}\|v\|_H^2 &= 2(1-\tau_l^{(2)}) v_1^{(1)} v_1^{(2)} - 2(1+\tau_r^{(2)}) v_m^{(1)} v_m^{(2)} \\ &- 2\tau_l^{(1)} v_1^{(1)} v_1^{(1)} - 2\tau_r^{(1)} v_m^{(1)} v_m^{(1)} + v^T(|A| \otimes S)v^T \, . \end{aligned}$$

In the last step Definition 2.7 is used. Stability follows if $\tau_l^{(2)} = 1$, $\tau_r^{(2)} = -1$ and $\tau_{l,r}^{(1)} \geq 0$, such that

$$\frac{d}{dt}\|v\|_H^2 = -2\tau_l^{(1)}(v_1^{(1)})^2 - 2\tau_r^{(1)}(v_m^{(1)})^2 + v^T(|A| \otimes S)v^T \leq 0 \, .$$

□

The upwind SBP operators thus introduce an artificial dissipation term $v^T(|A| \otimes S)v^T$. The stability analysis with a traditional SBP operator (simply replace $D_\pm$ by D_1 every where) results in the following energy estimate

$$\frac{d}{dt}\|v\|_H^2 = -2\tau_l^{(1)}(v_1^{(1)})^2 - 2\tau_r^{(1)}(v_m^{(1)})^2 \, .$$

Remark The "free" SAT parameters $\tau_{l,r}^{(1)} = \tau^{(1)}$ in lemma 3.1 strongly affect the numerical efficiency (referring to spectral radius and accuracy). A careful numerical study show (although not presented here) that the optimal value is given by $\tau^{(1)} = -1$. This is the value chosen in the numerical computations of (25).

The CFL number dt/h, where dt is the time-step and h the spatial grid-step when time-stepping the ODE system given by (25) is proportional to the spectral radius of $P\,h$, where

$$P = (A_+ \otimes D_+) + (A_- \otimes D_-) + \tau_l \otimes H^{-1} e_1 e_1^T + \tau_r \otimes H^{-1} e_m e_m^T \, .$$

The eigenvalues of $P\,h$, employing both traditional and upwind SBP operators are presented in Figure 1, where $m = 51$. In table 2 the corresponding spectral radii are presented.

Operator	p=2	p=4	p=6	p=8
traditional (order p)	1.00	1.37	1.80	1.72
upwind (order p)	4.10	2.61	2.02	2.07
upwind (order p+1)	1.53	1.61	1.70	1.92

Table 2: The spectral radius of $P\,h$ for the various SBP discretisations of (25).

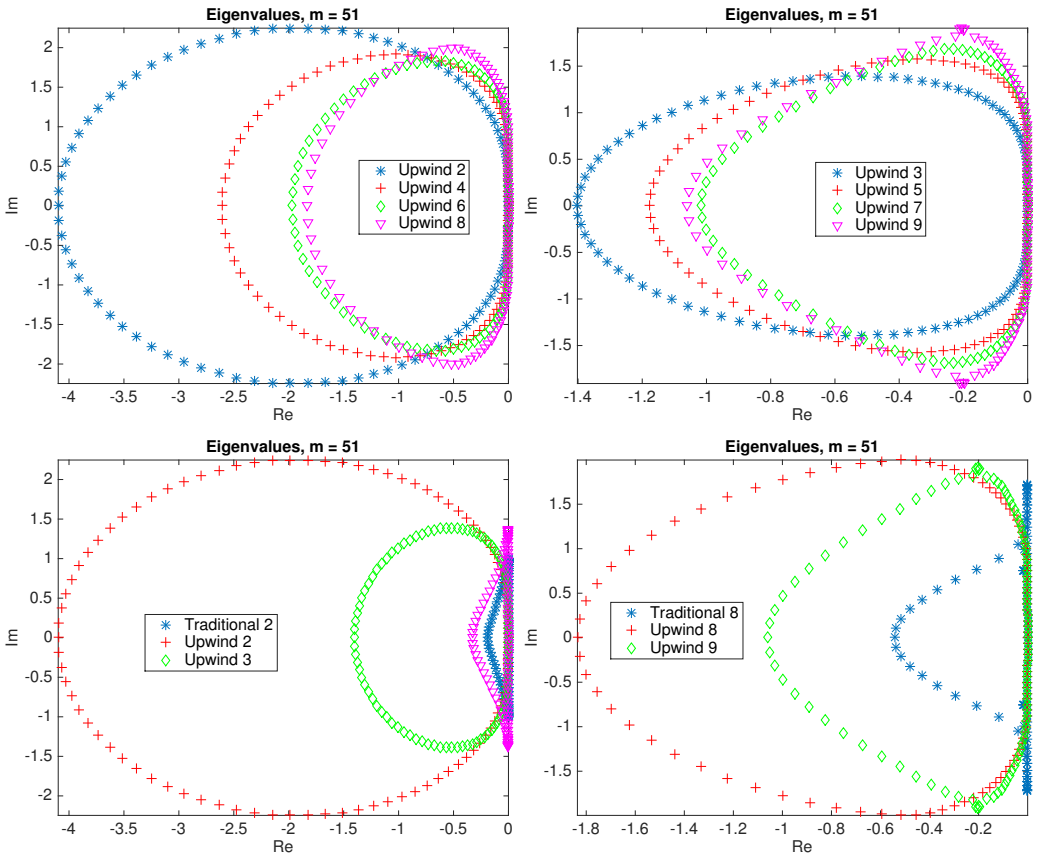

Figure 1: Comparing the eigenvalues of $P\,h$ for the various SBP discretisations of (25).

3.3 Second order hyperbolic systems

Consider the second order wave equation on piecewise continuous media,

$$\begin{array}{lll}
a^{(l)}u_{tt}^{(l)} = (b^{(l)}u_x^{(l)})_x, & -1 \le x \le 0, & t \ge 0 \\
a^{(r)}u_{tt}^{(r)} = (b^{(r)}u_x^{(r)})_x, & 0 \le x \le 1, & t \ge 0 \\
b^{(l)}u_x^{(l)} = b^{(r)}u_x^{(r)}\ , u^{(l)} = u^{(r)}, & x = 0, & t \ge 0 \\
u_x^{(l)} = 0, & x = -1, & t \ge 0 \\
u_x^{(r)} = 0, & x = 1, & t \ge 0 \\
u^{(l)} = f^{(l)},\ u_t^{(l)} = 0, & -1 \le x \le 0, & t = 0 \\
u^{(r)} = f^{(r)},\ u_t^{(r)} = 0, & 0 \le x \le 1, & t = 0
\end{array} \quad , \tag{26}$$

where $a^{(l)} \neq a^{(r)}$, $b^{(l)} \neq b^{(r)}$. Here $u^{(l,r)}$ denote the solutions corresponding to the left and right domains respectively, and $f^{(l,r)}$ the corresponding initial data. (A detailed analysis of this particular problem is described in [17].) The following coordinate transformations,

$$\begin{array}{ll}
x = x(\xi) = \xi \left(\frac{e^{-(\xi+\frac{4}{5})^2}}{e^{-(-1+\frac{4}{5})^2}} \right)^l, & \xi \in [-1, 0]\ , \\
x = x(\xi) = \xi \left(\frac{e^{-(\xi-\frac{4}{5})^2}}{e^{-(1-\frac{4}{5})^2}} \right)^l, & \xi \in [0, 1]\ ,
\end{array} \tag{27}$$

are introduced in the left and right domains, respectively. Here l is a non-negative integer, where the case $l = 0$ corresponds to the Cartesian case. A larger value of l leads to a denser clustering of grid-points close to the interface and the outer boundaries. The problem (26) transforms to

$$\begin{array}{lll}
\tilde{a}^{(l)}u_{tt}^{(l)} = (\tilde{b}^{(l)}u_\xi^{(l)})_\xi, & -1 \le \xi \le 0, & t \ge 0 \\
\tilde{a}^{(r)}u_{tt}^{(r)} = (\tilde{b}^{(r)}u_\xi^{(r)})_\xi, & 0 \le \xi \le 1, & t \ge 0 \\
\tilde{b}^{(l)}u_\xi^{(l)} = \tilde{b}^{(r)}u_\xi^{(r)}\ , u^{(l)} = u^{(r)}, & \xi = 0, & t \ge 0 \\
u_\xi^{(l)} = 0, & \xi = -1, & t \ge 0 \\
u_\xi^{(r)} = 0, & \xi = 1, & t \ge 0 \\
u^{(l)} = f^{(l)},\ u_t^{(l)} = 0, & -1 \le \xi \le 0, & t = 0 \\
u^{(r)} = f^{(r)},\ u_t^{(r)} = 0, & 0 \le \xi \le 1, & t = 0
\end{array} \quad , \tag{28}$$

in curvilinear coordinates, where $\tilde{a}^{(l,r)} = a^{(l,r)}x_\xi^{(l,r)}$ and $\tilde{b}^{(l,r)} = b^{(l,r)}/x_\xi^{(l,r)}$.

The semi-discrete approximation of the continuity conditions $u^{(l)} = u^{(r)}$ and $\tilde{b}^{(l)}u_\xi^{(l)} = \tilde{b}^{(r)}u_\xi^{(r)}$ can be written,

$$I_1 \equiv e_m^T v^{(l)} - e_1^T v^{(r)} = 0\ , \quad I_2 \equiv \tilde{b}_m^{(l)} e_m d_{1;\,m} v^{(l)} - \tilde{b}_1^{(r)} e_1 d_{1;\,1} v^{(r)} = 0 \quad , \tag{29}$$

where $v^{(l,r)}$ are the solution vectors corresponding to the left and right domains respectively, and $\tilde{b}^{(l,\,r)}_{1,\,m}$ the boundary values of $\tilde{b}^{l,\,r}(\xi)$, at the interface. The left and right domains are discretized using m grid points.

Let $\tilde{D}_2^{(a)}$ denote either a traditional or upwind (diagonal-norm) second derivative SBP operator. The SBP-SAT method for (28) is given by,

$$\begin{aligned}
\tilde{A}^{(l)}v_{tt}^{(l)} &= \tilde{D}_2^{(\tilde{b}^{(l)})}v^{(l)} & \tilde{A}^{(r)}v_{tt}^{(2)} &= \tilde{D}_2^{(\tilde{b}^{(r)})}v^{(r)} \\
&+\tau H^{-1}e_m(I_1) & &-\tau H^{-1}e_1(I_1) \\
&+\beta H^{-1}\tilde{b}_m^{(l)}d_{1;\,m}^T(I_1) & &-\beta H^{-1}\tilde{b}_1^{(r)}d_{1;\,1}^T(I_1) \qquad . \qquad (30)\\
&+\gamma H^{-1}e_m(I_2) & &-\gamma H^{-1}e_1(I_2) \\
&-H^{-1}\tilde{b}_1^{(l)}e_1d_{1;\,1}v^{(l)} & &+H^{-1}\tilde{b}_m^{(r)}e_md_{1;\,m}v^{(r)}
\end{aligned}$$

The following Lemma was first stated in [17]:

Lemma 3.2 *The scheme (30) is stable if $\tilde{D}_2^{(\tilde{b}^{(l,\,r)})}$ are diagonal-norm SBP operators and $\gamma = -\frac{1}{2}$, $\beta = \frac{1}{2}$, and $\tau \leq -\frac{\tilde{b}^{(l)}+\tilde{b}^{(r)}}{4\alpha_1\, h}$ hold.*

The proof can be found in [17]. The values for α_1 utilizing the second derivative upwind SBP operators is given by the first and last boundary elements (h_1 and h_m) in the norm matrix H (see Appendix).

4 Computations

4.1 First order hyperbolic system

Consider the hyperbolic system, defined by (20) and (23). The accuracy of the SBP-SAT approximation (25) will be verified against an analytic solution, where a narrow Gaussian pulse is propagated and reflected at the boundaries.

The following Gaussian profiles,

$$\theta^{(1)}(x,t) = \exp\left(-\frac{x-t}{r_*}\right)^2 \quad , \quad \theta^{(2)}(x,t) = -\exp\left(-\frac{x-t}{r_*}\right)^2 ,$$

are introduced where r_* defines the width of the Gaussian. Let $L = x_r - x_l$ denote the width of the domain. The initial data is set to: $u_t^{(1)}(x,0) = 0$, $u_t^{(2)}(x,0) = 0$, and

$$u^{(1)}(x,0) = \theta^{(2)}(x,0) - \theta^{(1)}(x,0)\,, \quad u^{(2)}(x,0) = \theta^{(2)}(x,0) + \theta^{(1)}(x,0)\,.$$

The analytic solution of (20) and (23) with the above provided initial data is given by,

$$u^{(1)}(x,t) = \theta^{(1)}(x, L-t) - \theta^{(2)}(x, L-t)\,, \quad u^{(2)}(x,t) = \theta^{(1)}(x, L-t) + \theta^{(2)}(x, L-t)\,,$$

after the Gaussian pulses have been reflected at the boundaries, i.e., when $t \in [L - L/4,\ L + L/4]$. In the numerical simulations (see Figure 2) $r_* = 0.1$ and $x_l = -1$, $x_r = 1$. The numerical approximations are integrated to $t = 1.8$ using the $4th$ order Runge-Kutta method, with a time step $dt = 0.01\ h$. (There is little difference between the time-step restrictions using the traditional and upwind SBP operators.) The waves reach the boundaries around $t = 0.9$. In Tables 3, 4 and 5 the convergence results using the traditional and upwind SBP operators (both even and odd orders) are compared.

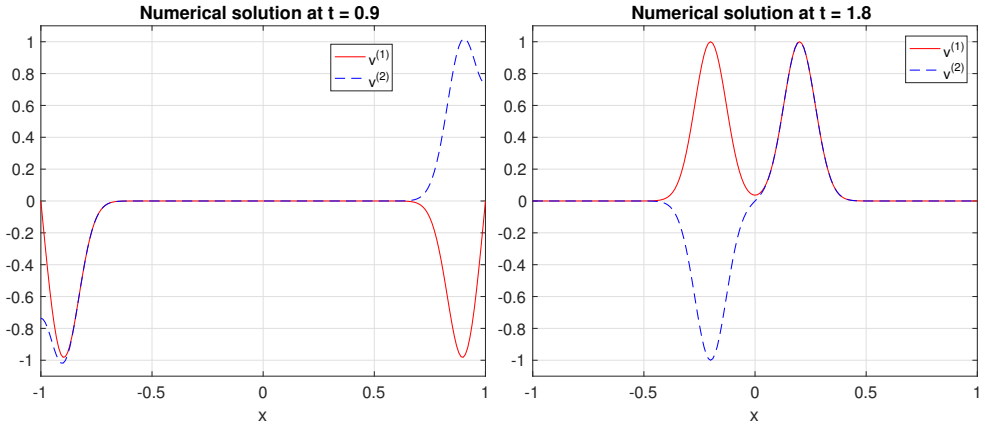

Figure 2: The numerical solutions at $t = 0.9$ and $t = 1.8$, solving (25), using the $9th$ order upwind SBP operator. Here $m = 201$.

m	$\log l^2{}_{(2nd)}$	q	$\log l^2{}_{(4th)}$	q	$\log l^2{}_{(6th)}$	q	$\log l^2{}_{(8th)}$	q
51	-0.29	0.00	-0.76	0.00	-1.09	0.00	-0.91	0.00
101	-0.59	1.00	-1.68	3.05	-2.00	3.04	-2.14	4.06
201	-1.10	1.69	-2.81	3.79	-3.11	3.69	-4.09	6.50
401	-1.69	1.96	-3.89	3.58	-4.29	3.91	-5.54	4.82
801	-2.29	2.00	-4.88	3.27	-5.49	3.98	-6.98	4.78

Table 3: $log(l_2 - errors)$ and convergence rates solving (25) using different traditional SBP operators.

m	$\log l^2{}_{(2nd)}$	q	$\log l^2{}_{(4th)}$	q	$\log l^2{}_{(6th)}$	q	$\log l^2{}_{(8th)}$	q
51	-0.33	0.00	-0.87	0.00	-1.24	0.00	-1.29	0.00
101	-0.50	0.57	-1.63	2.50	-2.71	4.90	-2.98	5.61
201	-0.86	1.20	-2.74	3.68	-4.49	5.90	-5.53	8.48
401	-1.40	1.78	-3.92	3.95	-6.23	5.78	-8.40	9.54
801	-1.99	1.97	-5.12	3.98	-8.00	5.88	-11.03	8.73

Table 4: $log(l_2 - errors)$ and convergence rates solving (25) using different even order upwind SBP operators.

m	$\log l^2{}_{(3rd)}$	q	$\log l^2{}_{(5th)}$	q	$\log l^2{}_{(7th)}$	q	$\log l^2{}_{(9th)}$	q
51	-0.72	0.00	-1.10	0.00	-1.24	0.00	-1.31	0.00
101	-1.24	1.73	-2.20	3.66	-2.76	5.05	-2.96	5.49
201	-2.00	2.53	-3.65	4.82	-4.83	6.90	-5.41	8.15
401	-2.87	2.90	-5.15	5.00	-6.96	7.05	-8.06	8.80
801	-3.77	2.98	-6.66	5.01	-9.07	7.04	-10.76	8.95

Table 5: $log(l_2 - errors)$ and convergence rates solving (25) using different odd order upwind SBP operators.

Remark The convergence results presented in Tables 4 and 5 show higher than expected convergence rates (see the previous remark in Section 2.3). This unexpected behaviour is also seen in Tables 7 and 8, for a second order hyperbolic problem. This is something to address in a coming study.

4.2 Second order hyperbolic problem

The accuracy of the discontinuous media treatment with the SBP-SAT method, given by (30) will be verified against an analytic solution. A narrow Gaussian pulse is propagated across the discontinuous media interface to verify the accuracy of the transmission and reflection properties at the interface. The initial data is given by

$$u(x,0) = \exp\left(-\tfrac{(x_0-x)^2}{r_0^2}\right), \quad u_t(x,0) = 0\ ,$$

where x_0 determines the position and r_0 determines the width of the Gaussian profile. In the present study $x_0 = -\frac{1}{4}$ and $r_0 = \frac{1}{30}$. Hence, the initial Gaussian profile is centred at $x = -0.25$ in the left sub-domain where the media parameters are given by $a^{(l)}$, $b^{(l)}$. The speed of sound and the acoustic impedance in the left and right subdomains are given by $c^{(l,r)} = \sqrt{\frac{a^{(l,r)}}{b^{(l,r)}}}$,

$\sigma^{(l,r)} = \sqrt{a^{(l,r)}\, b^{(l,r)}}$. For $t > 0$ the initial Gaussian profile splits into one left-going and one right-going Gaussian wave (see Figure 3) propagating with speed $c^{(l)}$, i.e., the analytic solution is given by

$$u(x,t) = \frac{1}{2}\exp\left(-\frac{(x_0-(x+c^{(l)}t))^2}{r_0^2}\right) + \frac{1}{2}\exp\left(-\frac{(x_0-(x-c^{(l)}t))^2}{r_0^2}\right),$$

assuming that the waves have not yet reached the left boundary or the interface. At $t_* = \frac{-x_0}{c^{(l)}}$ (in the present study $t_* = 0.25$), the right-going wave hits the media interface at $x = 0$ and splits into a reflected wave and a transmitted wave, see Figure 3. The transmission (T) and reflection (R) coefficients are given by

$$T = \tfrac{2\,\sigma^{(l)}}{\sigma^{(l)}+\sigma^{(r)}}, \quad R = \tfrac{\sigma^{(l)}-\sigma^{(r)}}{\sigma^{(l)}+\sigma^{(r)}}\ .$$

Hence, at $t > t_*$ the analytic solution consists of a left-going wave (with speed $c^{(l)}$ and amplitude $\frac{1}{2}$) from the initial condition, a reflected wave with amplitude $\frac{R}{2}$ moving (with speed $c^{(l)}$) to the left from the interface at $x = 0$, and a transmitted right-going wave with amplitude $\frac{T}{2}$ propagating with speed $c^{(r)}$. The analytic solution is given by

$$\begin{array}{ll} u^{(l)} = \frac{1}{2}\exp\left(-\frac{(x_0-(x+c^{(l)}t))^2}{r_0^2}\right) + \frac{R}{2}\exp\left(-\frac{(x+c^{(l)}(t-t_*))^2}{r_0^2}\right) & x \in [-1,0], \\ u^{(r)} = \frac{T}{2}\exp\left(-\frac{(c^{(l)}(x-c^{(r)}(t-t_*)))^2}{(c^{(r)}r_0)^2}\right), & x \in [0,1]\ , \end{array} \tag{31}$$

assuming that left-going and right-going waves have not yet reached the outer boundaries.

In the numerical simulations $a^{(l)} = 1$, $b^{(l)} = 1$, $a^{(r)} = 2$ and $b^{(r)} = 8$ are chosen. A curvilinear grid is used by setting $l = 2$ in (27). At the outer boundaries homogeneous Neumann boundary conditions are imposed. The numerical approximations are integrated to $t = 0.5$ using the $4th$ order Runge-Kutta method, with a time step $dt = 0.05\ h$. (There is little difference between the time-step restrictions using the traditional and upwind SBP operators.) In Tables 6, 7 and 8 the results using the traditional and upwind SBP operators are compared.

m	$\log l^2{}_{(2nd)}$	q	$\log l^2{}_{(4th)}$	q	$\log l^2{}_{(6th)}$	q
51	-1.16	0.00	-1.47	0.00	-1.67	0.00
101	-1.50	1.13	-2.23	2.56	-2.78	3.74
201	-2.02	1.74	-3.36	3.77	-4.45	5.58
401	-2.61	1.98	-4.55	3.97	-6.22	5.91
801	-3.21	2.00	-5.75	3.99	-8.02	5.98

Table 6: $log(l_2 - errors)$ and convergence rates solving (30) using different traditional SBP operators. On a grid defined by (27) with $l = 2$.

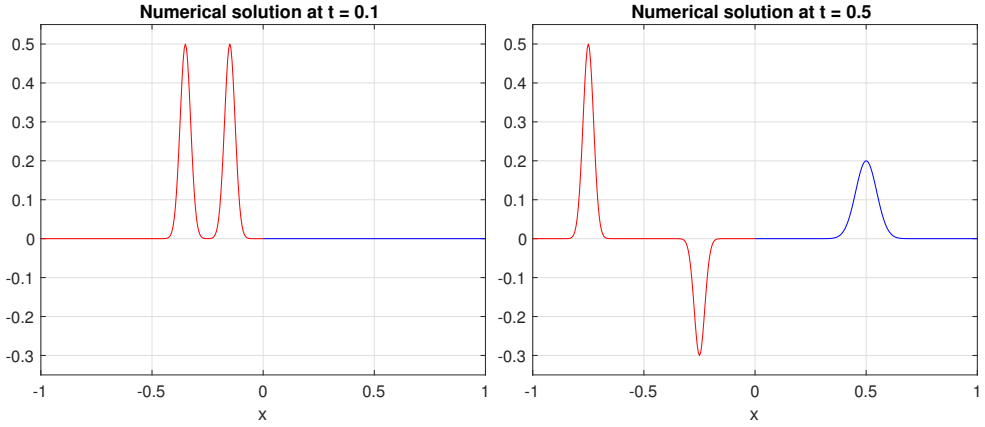

Figure 3: The numerical solutions at $t = 0.1$ and $t = 0.5$, solving (30) on a grid defined by (27) with $l = 2$ and $m = 201$, using the $5th$ order upwind SBP operator.

m	$\log l^2{}_{(2nd)}$	q	$\log l^2{}_{(4th)}$	q	$\log l^2{}_{(6th)}$	q	$\log l^2{}_{(8th)}$	q
51	-0.92	0.00	-1.19	0.00	-1.67	0.00	-1.74	0.00
101	-0.99	0.24	-1.64	1.54	-2.26	2.01	-2.83	3.64
201	-1.30	1.02	-2.50	2.86	-3.55	4.30	-4.45	5.43
401	-1.74	1.48	-3.62	3.73	-5.22	5.57	-6.66	7.36
801	-2.31	1.89	-4.80	3.94	-6.99	5.90	-9.02	7.85

Table 7: $log(l_2 - errors)$ and convergence rates solving (30) using different even order upwind SBP operators. On a grid defined by (27) with $l = 2$.

m	$\log l^2{}_{(3rd)}$	q	$\log l^2{}_{(5th)}$	q	$\log l^2{}_{(7th)}$	q	$\log l^2{}_{(9th)}$	q
51	-1.19	0.00	-1.31	0.00	-1.46	0.00	-1.49	0.00
101	-1.68	1.66	-2.07	2.57	-2.39	3.14	-2.66	3.95
201	-2.61	3.11	-3.55	4.97	-4.38	6.65	-5.11	8.20
401	-3.78	3.89	-5.32	5.87	-6.71	7.77	-8.00	9.63
801	-4.97	3.98	-7.11	5.97	-9.10	7.94	-10.86	9.52

Table 8: $log(l_2 - errors)$ and convergence rates solving (30) using different odd order upwind SBP operators. On a grid defined by (27) with $l = 2$.

5 Analysis in 2D

5.1 Definitions

The following definition will be used in subsequent sections:

Definition 5.1 *Let $\bar{x} = (x, y)$ denote grid coordinates in two dimensions. Denote the 2D bounding box $x_l \leq x \leq x_r,\ y_b \leq y \leq y_t$ by $\bar{x} \in \Omega$, and the line $x = x_r,\ y_b \leq y \leq y_t$ by $\bar{x} \in \delta\Omega_{East}$. A grid-function u restricted to $\bar{x} \in \delta\Omega_{East}$ will be denoted u_E.*

The domain Ω is discretized with an $(m_x+1)\times(m_y+1)$-point equidistant grid defined as

$$\begin{aligned} x_i &= x_l + (i-1)h_x, \quad i = 0, 1, \ldots, m_x, \quad h_x = \tfrac{x_r - x_l}{m_x - 1}, \\ y_j &= y_b + (j-1)h_y, \quad j = 0, 1, \ldots, m_y, \quad h_y = \tfrac{y_t - y_b}{m_y - 1}. \end{aligned}$$

In the following, k denotes the number of unknowns in the underlying continuous PDE. The numerical approximation at grid point $(x_i,\, y_j) \equiv \bar{x}_{i,j}$ is a $1 \times k$-vector denoted $v_{i,j}$. The tensor product derivations are more transparent by redefining the component vector $v_{i,j}$ as a "vector of vectors." Specifically, define a discrete solution vector $v^T = [v^1, v^2, \ldots, v^{m_x}]$, where $v^p = [v_{p,1}, v_{p,2}, \ldots, v_{p,m_y}]$ is the solution vector at x_p along the y-direction, see Figure 4. To distinguish whether a 2D difference operator P is operating in the x- or the y-direction, the notations P_x and P_y is used, respectively. The following 2D operators are frequently used:

$$\begin{array}{llll} D_x & = I_k \otimes D_1 \otimes I_{m_y}, & D_y & = I_k \otimes I_{m_x} \otimes D_1 \\ D_{x-} & = I_k \otimes D_- \otimes I_{m_y}, & D_{y-} & = I_k \otimes I_{m_x} \otimes D_- \\ D_{x+} & = I_k \otimes D_+ \otimes I_{m_y}, & D_{y+} & = I_k \otimes I_{m_x} \otimes D_+ \\ S_x & = I_k \otimes S \otimes I_{m_y}, & S_y & = I_k \otimes I_{m_x} \otimes S \\ B_x & = I_k \otimes B \otimes I_{m_y}, & B_y & = I_k \otimes I_{m_x} \otimes B \\ H_x & = I_k \otimes H \otimes I_{m_y}, & H_y & = I_k \otimes I_{m_x} \otimes H \\ e_{West} & = I_k \otimes e_1 \otimes I_{m_y}, & e_{South} & = I_k \otimes I_{m_x} \otimes e_1 \\ e_{East} & = I_k \otimes e_{m_x} \otimes I_{m_y}, & e_{North} & = I_k \otimes I_{m_x} \otimes e_{m_y} \end{array}, \tag{32}$$

where D_1, D_-, D_+, S, B and H are the 1-D operators introduced in Section 2. I_{m_x}, I_{m_y} and I_k are identity matrices of appropriate sizes, and e_1, e_{m_x} and e_{m_y} are 1D "boundary" vectors defined by (1). Further introduce the 2D norm operators $\tilde{H} = H_x H_y$, and $\hat{H} = I_2 \otimes \tilde{H}$. To simplify notation further introduce $v_W = e_{West}^T v$, $v_E = e_{East}^T v$, $v_S = e_{South}^T v$, $v_N = e_{North}^T v$.

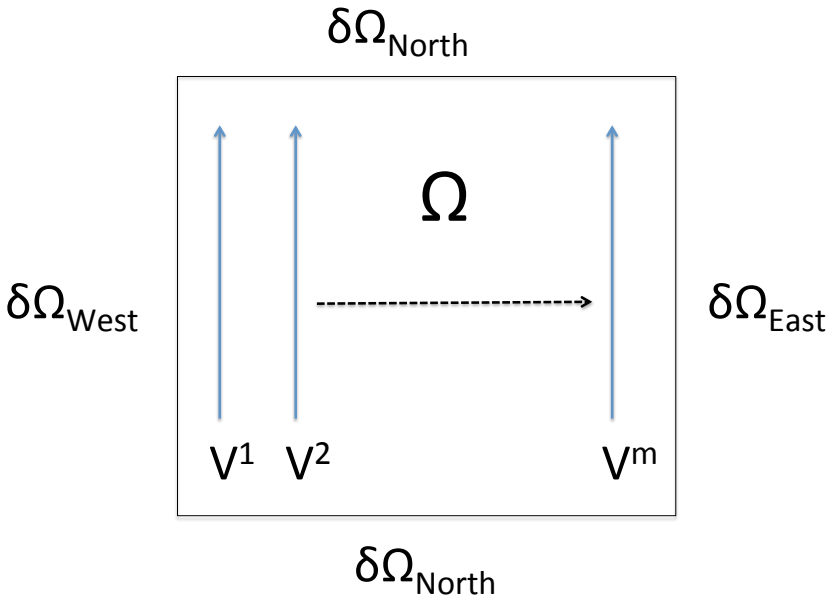

Figure 4: Notation for the computational domain in 2D.

Two following 2D relations are useful in the coming 2D semi-discrete analysis,

$$\begin{array}{l}(H_x \otimes H_y)(D_- \otimes D_+) = (-D_+ \otimes I_{m_x})^T (H_x \otimes H_y)(I_{m_y} \otimes D_+) = -(D_{x+})^T \tilde{H} D_{y+} \\ (H_x \otimes H_y)(D_+ \otimes D_-) = (-D_- \otimes I_{m_x})^T (H_x \otimes H_y)(I_{m_y} \otimes D_-) = -(D_{x-})^T \tilde{H} D_{y-}\end{array} .$$

5.2 Parabolic systems

Consider the 2D hyperbolic-parabolic system (with k unknowns):

$$\mathbf{u}_t = \mathbf{A_1 u}_x + \mathbf{A_2 u}_y + \left(\mathbf{C_{11} u}_x + \mathbf{C_{12} u}_y\right)_x + \left(\mathbf{C_{21} u}_x + \mathbf{C_{22} u}_y\right)_y \ , \ \bar{x} \in \Omega. \quad (33)$$

To simplify notation introduce,

$$\mathbf{C} = \begin{bmatrix} \mathbf{C_{11}} & \mathbf{C_{12}} \\ \mathbf{C_{21}} & \mathbf{C_{22}} \end{bmatrix} \ , \hat{\mathbf{u}} = \begin{bmatrix} \mathbf{u}_x \\ \mathbf{u}_y \end{bmatrix} .$$

Parabolicity requires that $(\mathbf{C} + \mathbf{C}^T)$ is positive semidefinite.

Consider the following boundary conditions at the 4 boundaries (East, West, North, South):

$$\begin{array}{l} \Phi_{East}\mathbf{u} + \mathbf{C_{11} u}_x + \mathbf{C_{12} u}_y = \mathbf{g}, \ \bar{x} \in \Omega_{East} \\ \Phi_{West}\mathbf{u} - \mathbf{C_{11} u}_x - \mathbf{C_{12} u}_y = \mathbf{g}, \ \bar{x} \in \Omega_{West} \\ \Phi_{North}\mathbf{u} + \mathbf{C_{21} u}_x + \mathbf{C_{22} u}_y = \mathbf{g}, \ \bar{x} \in \Omega_{North} \\ \Phi_{South}\mathbf{u} - \mathbf{C_{21} u}_x - \mathbf{C_{22} u}_y = \mathbf{g}, \ \bar{x} \in \Omega_{South} \ , \end{array} \quad (34)$$

here assuming that (33) is completely parabolic (see for example [18]).

Remark Other types of well-posed boundary conditions, like Dirichlet can also be imposed. However, the main focus in the present study is the derivation of upwind SBP operators. The analysis of the boundary treatment with SAT is independent of the type of SBP operator employed. For a detailed analysis how to impose BC using SBP-SAT for the compressible Navier-Stokes equations (which is an incompletely parabolic system) see for example [26, 34, 35].

Multiplying Eq. 33 by $\mathbf{u}^T$, and integrating by parts with the use of (34) lead to

$$\frac{d}{dt}\|\mathbf{u}\|^2 = BT_{East} + BT_{West} + BT_{North} + BT_{South} + DI \ , \tag{35}$$

where the diffusion (or dissipation) DI is given by,

$$DI = -\int\int_{\Omega} \hat{\mathbf{u}}^T \left[\mathbf{C} + \mathbf{C}^T\right] \hat{\mathbf{u}} \, dx \, dy, \tag{36}$$

and the boundary terms,

$$\begin{array}{l} BT_{East} = -\int_{\partial\Omega_{East}} \mathbf{u}^T \left((2\mathbf{\Phi}_{East} - \mathbf{A_1})\mathbf{u} - \mathbf{g}\right) \, dy \ , \\ BT_{West} = -\int_{\partial\Omega_{West}} \mathbf{u}^T \left((2\mathbf{\Phi}_{West} + \mathbf{A_1})\mathbf{u} - \mathbf{g}\right) \, dy \ , \\ BT_{North} = -\int_{\partial\Omega_{North}} \mathbf{u}^T \left((2\mathbf{\Phi}_{North} - \mathbf{A_2})\mathbf{u} - \mathbf{g}\right) \, dx \ , \\ BT_{South} = -\int_{\partial\Omega_{South}} \mathbf{u}^T \left((2\mathbf{\Phi}_{South} + \mathbf{A_2})\mathbf{u} - \mathbf{g}\right) \, dx \ . \end{array} \tag{37}$$

An energy estimate exists if

$$\begin{array}{ll} 2\mathbf{\Phi}_{East} - \mathbf{A_1} \geq 0 \ , & 2\mathbf{\Phi}_{West} + \mathbf{A_1} \geq 0 \\ 2\mathbf{\Phi}_{North} - \mathbf{A_2} \geq 0 \ , & 2\mathbf{\Phi}_{South} + \mathbf{A_2} \geq 0 \end{array} \ . \tag{38}$$

Let $\mathbf{A_1} = \mathbf{A_{1+}} + \mathbf{A_{1-}}$ and $\mathbf{A_2} = \mathbf{A_{2+}} + \mathbf{A_{2-}}$ denote *Steger-Warming* flux splitting of $\mathbf{A_1}$ and $\mathbf{A_2}$, respectively. (This was defined in Section 3.1 for the 1D case.) A well-posed set of BC (34) is given by choosing

$$\begin{array}{ll} \mathbf{\Phi}_{East} = \mathbf{A_{1+}} \ , & \mathbf{\Phi}_{West} = \mathbf{A_{1-}} \\ \mathbf{\Phi}_{North} = \mathbf{A_{2+}} \ , & \mathbf{\Phi}_{South} = \mathbf{A_{2-}} \end{array} \ . \tag{39}$$

Remark For the purely hyperbolic case, i.e., if the viscous terms are removed (by setting $\mathbf{C}$ to zero), a well-posed set of boundary conditions is given by (34) with the choice presented in (39). This particular choice is often referred to as characteristic BC (see for example [36, 21, 15]). In the coming section characteristic BC for the compressible Euler equations will be utilized.

An SBP-SAT approximation of (33) on flux-splitted form using the upwind SBP operators, with the boundary conditions (34) is given by,

$$\begin{aligned} v_t &= D_{x+}A_{1+}v + D_{x-}A_{1-}v + D_{y+}A_{2+}v + D_{y-}A_{2-}v \\ &+ D_{x+}\left(C_{11}D_{x-} + C_{12}D_{y-}\right)v + D_{y+}\left(C_{21}D_{x-} + C_{22}D_{y-}\right)v + SAT_{E-,W-,N-,S-} \ , \end{aligned} \tag{40}$$

where $SAT_{E-,W-,N-,S-}$ impose the boundary conditions (34) using the penalty technique,

$$\begin{aligned} SAT_{E-} &= -\tau_E H_x^{-1} e_{East}\left((\Phi_{East}v + C_{11}D_{x-}v + C_{12}D_{y-}v)_E - g\right) \ , \\ SAT_{W-} &= -\tau_W H_x^{-1} e_{West}\left((\Phi_{West}v - C_{11}D_{x-}v - C_{12}D_{y-}v)_W - g\right) \ , \\ SAT_{N-} &= -\tau_N H_y^{-1} e_{North}\left((\Phi_{North}v + C_{21}D_{x-}v + C_{22}D_{y-}v)_N - g\right) \ , \\ SAT_{S-} &= -\tau_S H_y^{-1} e_{South}\left((\Phi_{South}v - C_{21}D_{x-}v - C_{22}D_{y-}v)_S - g\right) \ . \end{aligned}$$

Here τ_E, τ_W, τ_N and τ_S are penalty parameters that will be tuned to obtain a semi-discrete energy estimate. In the following, the subscripts E, W, N, S indicate that the quantities reside on the East, West, North and South boundaries (see Figure 4). So simplify notation introduce,

$$\hat{C} = \begin{bmatrix} C_{11} & C_{12} \\ C_{21} & C_{22} \end{bmatrix} \ , \hat{v_-} = \begin{bmatrix} D_{x-}v \\ D_{y-}v \end{bmatrix} .$$

Apply the energy method by multiplying (40) by $v^T\tilde{H}$, and adding the transpose, leading to

$$\frac{d}{dt}\|v\|_{\tilde{H}}^2 = BT_{E-} + BT_{W-} + BT_{N-} + BT_{S-} + DI_{h-} + AD_h \ , \tag{41}$$

where the semi-discrete diffusion (or dissipation) DI_{h-} is given by

$$DI_{h-} = \hat{v_-}^T\hat{H}\hat{C}\hat{v_-} \ , \tag{42}$$

and the artificial dissipation $AD_h = v^T\left(|A_1|S_xH_y\right)v + v^T\left(|A_2|S_yH_x\right)v$. The boundary terms are given by,

$$\begin{aligned} BT_{E-} &= (1-\tau_E)v_E^T H_y\left(C_{11}D_{x-}v + C_{12}D_{y-}v\right)_E \\ &+(1-\tau_E)\left(C_{11}D_{x-}v + C_{12}D_{y-}v\right)_E^T H_y v_E + v_E^T H_y\left(A_1 - 2\tau_E\Phi_{East}\right)v_E \\ BT_{W-} &= -(1+\tau_E)v_E^T H_y\left(C_{11}D_{x-}v + C_{12}D_{y-}v\right)_W \\ &-(1+\tau_W)\left(C_{11}D_{x-}v + C_{12}D_{y-}v\right)_W^T H_y v_W - v_W^T H_y\left(A_1 + 2\tau_W\Phi_{West}\right)v_W \\ BT_{N-} &= (1-\tau_N)v_N^T H_x\left(C_{21}D_{x-}v + C_{22}D_{y-}v\right)_N \\ &+(1-\tau_N)\left(C_{21}D_{x-}v + C_{22}D_{y-}v\right)_N^T H_x v_N + v_N^T H_x\left(A_2 - 2\tau_N\Phi_{North}\right)v_N \\ BT_{S-} &= -(1+\tau_S)v_E^T H_x\left(C_{21}D_{x-}v + C_{22}D_{y-}v\right)_S \\ &-(1+\tau_S)\left(C_{21}D_{x-}v + C_{22}D_{y-}v\right)_S^T H_x v_S - v_S^T H_y\left(A_2 + 2\tau_S\Phi_{South}\right)v_S \ . \end{aligned} \tag{43}$$

If $\tau_{E,W,N,S} = 1$, the semi-discrete boundary terms (43) exactly mimic the continuous boundary terms (37), and stability follows if (38) holds.

Remark An alternative SBP-SAT approximation to (40) is given by

$$\begin{aligned} v_t &= D_{x+}A_{1+}v + D_{x-}A_{1-}v + D_{y+}A_{2+}v + D_{y-}A_{2-}v \\ &+ D_{x-}\left(C_{11}D_{x+} + C_{12}D_{y+}\right)v + D_{y-}\left(C_{21}D_{x+} + C_{22}D_{y+}\right)v + SAT_{E+,W+,N+,S+} \ , \end{aligned} \tag{44}$$

where

$$\begin{aligned} SAT_{E+} &= -\tau_E H_x^{-1} e_{East}\left((\Phi_{East}v + C_{11}D_{x+}v + C_{12}D_{y+}v)_E - g\right) \ , \\ SAT_{W+} &= -\tau_W H_x^{-1} e_{West}\left((\Phi_{West}v - C_{11}D_{x+}v - C_{12}D_{y+}v)_W - g\right) \ , \\ SAT_{N+} &= -\tau_N H_y^{-1} e_{North}\left((\Phi_{North}v + C_{21}D_{x+}v + C_{22}D_{y+}v)_N - g\right) \ , \\ SAT_{S+} &= -\tau_S H_y^{-1} e_{South}\left((\Phi_{South}v - C_{21}D_{x+}v - C_{22}D_{y+}v)_S - g\right) \ . \end{aligned}$$

Stability follows if $\tau_{E,W,N,S} = 1$. The difference between (40) and (44) is merely the order in which you apply the upwind SBP operators in the viscous terms. The convective terms are identical.

Remark Employing traditional first derivative SBP operators for the problem given by (33) and (34) leads to (40) with D_+ and D_- replaced by D_1 everywhere. This means that

$$\hat{v_-} = \begin{bmatrix} D_{x-}v \\ D_{y-}v \end{bmatrix} ,$$

is replaced by

$$\hat{v} = \begin{bmatrix} D_x v \\ D_y v \end{bmatrix} \ ,$$

and that $AD_h = 0$. Hence, there is no longer any damping mechanism for the π-mode. The SBP-SAT scheme using D_1 is nevertheless linearly stable.

6 The Euler vortex problem

To test the accuracy of the novel upwind SBP operators, an Euler-vortex that satisfies the 2D Euler equations, under the assumption of isentropy is run across conforming multiblock interfaces. The problem setup consists of two blocks (10×10 unit area) having matching gridlines (see Figure 5). The two blocks (left and right) are patched together at both ends using the SBP-SAT method, i.e., the east boundary of the right block is coupled to the west boundary of the left block, and the east boundary of the left

block is coupled to the west boundary of the right block. Details concerning how to discretize this problem with the SBP-SAT method can be found in [36, 21, 15]. This cyclic SBP-SAT coupling makes it possible to simulate a long-time simulation of the Euler-vortex problem, where the vortex crosses multiple block-interfaces. This will allow us to verify both the long-time stability behaviour and the boundary accuracy, employing the novel upwind SBP operators.

The analytic vortex solution is steady in the frame of reference moving with the free-stream. Let $p_\infty = (\gamma\, M^2)^{-1}$ denote the nondimensional background pressure, where M is the Mach number and $\gamma = c_p/c_v = 1.4$ (in air). The scaled vortex has the velocity field

$$v_\Theta = \frac{\epsilon r}{2\pi\sqrt{p_\infty} r_*^2} \exp\left(\frac{1-r^2}{2\, r_*}\right), \tag{45}$$

where ϵ is the nondimensional circulation, r_* the nondimensional effective radius and (r, Θ) the the polar coordinates. The strength of the vortex is governed by the parameter ϵ and the size of the vortex is governed by the parameter r_*.

The analytic solution, in the nondimensionalized primitive variables: density (ρ), velocity in x-direction (u), velocity in y-direction (v) and pressure (p), in a fixed frame of reference (x, y, t) becomes,

$$\begin{aligned} u &= 1 - \tfrac{\epsilon y}{2\pi\sqrt{p_\infty} r_*^2} \exp\left(\tfrac{f(x,y,t)}{2}\right), & v &= \tfrac{\epsilon((x-x_0)-t)}{2\pi\sqrt{p_\infty} r_*^2} \exp\left(\tfrac{f(x,y,t)}{2}\right) \\ \rho &= \left(1 - \tfrac{\epsilon^2(\gamma-1)M^2}{8\pi^2 p_\infty r_*^2} exp\left(f(x,y,t)\right)\right)^{\frac{1}{\gamma-1}}, & p &= p_\infty \rho^\gamma \end{aligned}, \tag{46}$$

where $f(x,y,t) = \frac{1-\left(((x-x_0)-t)^2+y^2\right)}{r_*^2}$ and x_0 is the initial position of the vortex (in the x-direction). The vortex is introduced into the computational domain by using the analytic solution as boundary data and initial data. In the present study the Mach number is set to $M = 0.5$, and the nondimensional effective radius $r_* = 2$. The largest possible value on ϵ is the limit when ρ becomes negative in Eq. 46, i.e. $\epsilon \leq \sqrt{\frac{8\pi^2 p_\infty r_*^2}{(\gamma-1)M^2}} = 94.9928$ (with $M = 0.5$ $\gamma = 1.4$ and $r_* = 2$).

In the first test a convergence study is performed, comparing the upwind SBP operators against the traditional SBP operators. The results are presented in Tables 9, 10 and 11. The vortex is initiated at $(x, y) = (0, 0)$, centered in the left block, and then integrated using the 4th order accurate Runge-Kutta method to $t = 20$ using a CFL of 1/6. At $t = 20$ the vortex has propagated with the free-stream across the first block interface (the left to

right block-coupling) a distance of 10 units into the right block, see Figure 5. Here $\epsilon = 5$, a relatively weak vortex strength. For the second order upwind case it was necessary to lower the CFL to 1/8 instead of 1/6.

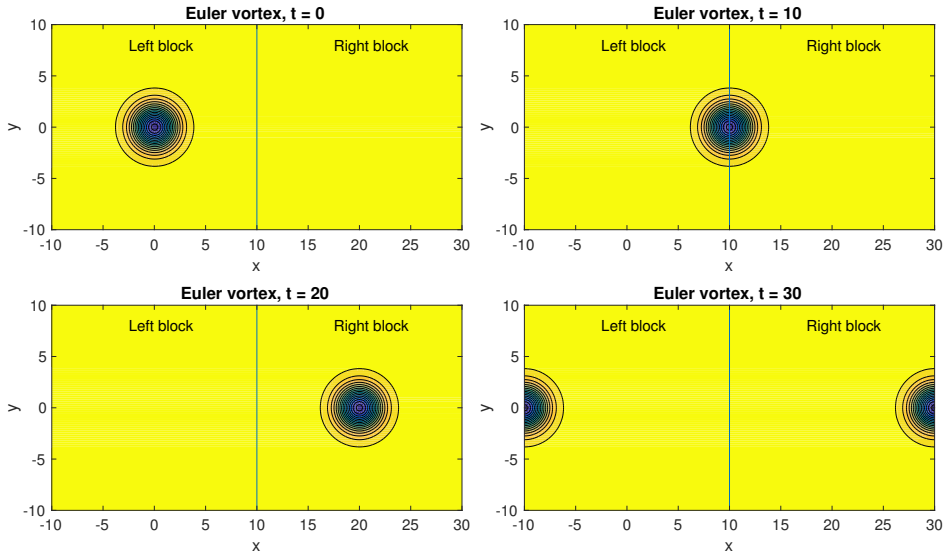

Figure 5: The setup for the two-block Euler vortex problem. Here $\epsilon = 5$ and $M = 0.5$. The vortex is initially centered at $(x, y) = (0, 0)$ and integrated using RK4. Here presenting the density contours. Employing the $9th$ order upwind method using 101^2 grid-points in each block. At $t = 10$ the vortex has propagated with the free-stream to the interface between the left and right block. At $t = 20$ it is centered in the right block. At $t = 30$ the vortex has reached the (cyclic) interface between the right and left block.

In the second test the long-time stability behaviour of the traditional and upwind SBP operators are compared. In Figure 6 long-time simulations (up to t=1000) with two different vortex strengths, $\epsilon = 5$ and $\epsilon = 20$ are presented, comparing the 9th order upwind SBP operator with the traditional 8th order SBP operator using 51^2 grid-points in each block. The vortex is initially centered at $(x, y) = (0, 0)$ and integrated using RK4 with a CFL of 1/6. The results indicate the robustness of the SBP-SAT discretisation using the 9th order upwind SBP operators.

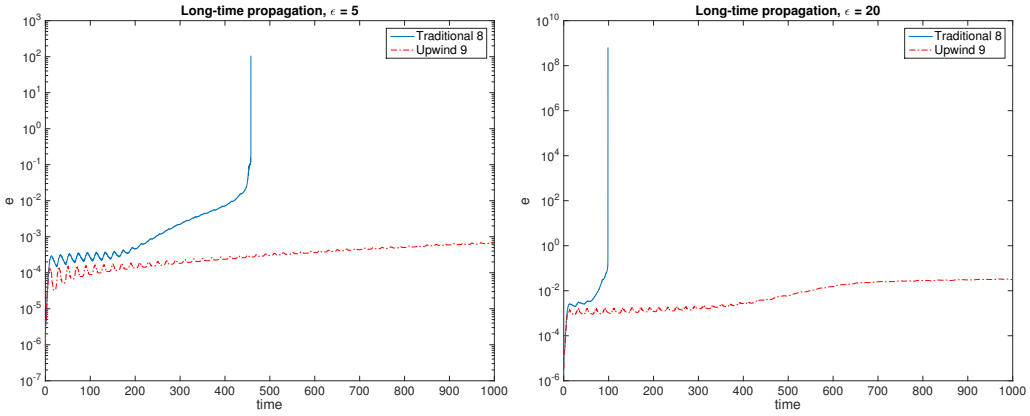

Figure 6: Comparing the long-time behaviour (l_2-error) of the traditional 8th order SBP and the 9th order upwind SBP operators for the Euler vortex problem with two vortex strengths: $\epsilon = 5$ (left) and $\epsilon = 20$ (right). The vortex is initially centered at $(x, y) = (0, 0)$ and integrated using RK4.

In the third and final test a very strong vortex with $\epsilon = 60$ using 51^2 grid-points in each block is initiated at $(x, y) = (0, 0)$. This is a much harder test since the problem is highly nonlinear due to the large vortex strength. Again the 9th order upwind SBP operator is compared with the traditional 8th order SBP operator. The results are presented in Figure 7. At $t = 15.1$ the solution using the traditional 8th order SBP operators becomes unstable, while the solution using the 9th order upwind SBP operators is very robust and accurate (here the solution is presented at $t = 200$).

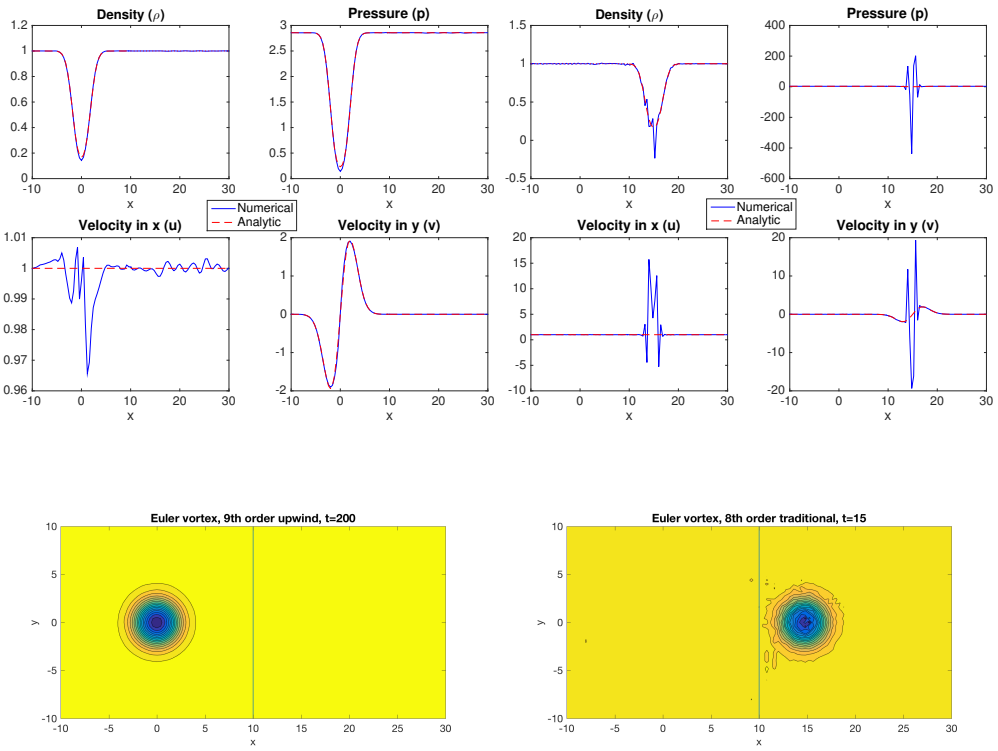

Figure 7: Comparing the traditional 8th order SBP (right column) and the 9th order upwind SBP (left column) operators for the Euler vortex problem where $\epsilon = 60$ (,i.e., a very powerful vortex). The vortex is initially centered at $(x, y) = (0, 0)$ and integrated using RK4 to t=15 (right) and t=200 (left). Top row: a cut along the center line ($y = 0$) for the four primitive variables (density, velocities and pressure). Bottom row: Density contours.

m	$\log l^2{}_{(2nd)}$	q	$\log l^2{}_{(4th)}$	q	$\log l^2{}_{(6th)}$	q	$\log l^2{}_{(8th)}$	q
51	-1.76	0.00	-3.08	0.00	-4.27	0.00	-4.49	0.00
101	-2.31	1.81	-4.39	4.37	-6.28	6.70	-6.76	7.55
201	-2.92	2.04	-5.66	4.20	-8.16	6.25	-9.24	8.24
301	-3.28	2.03	-6.37	4.07	-9.17	5.73	-10.17	5.26
401	-3.53	2.02	-6.87	4.03	-9.82	5.21	-10.73	4.49

Table 9: $log(l_2 - errors)$ and convergence rates using even-order upwind SBP operators, for the two-block Euler vortex problem. $\epsilon = 5$. Vortex initiated at $x = 0$ and integrated to $t = 20$, when the vortex has passed the interface.

m	$\log l^2{}_{(3rd)}$	q	$\log l^2{}_{(5th)}$	q	$\log l^2{}_{(7th)}$	q	$\log l^2{}_{(9th)}$	q
51	-2.21	0.00	-3.50	0.00	-4.38	0.00	-4.48	0.00
101	-3.02	2.67	-4.96	4.87	-6.45	6.88	-6.76	7.55
201	-3.90	2.93	-6.46	4.97	-8.49	6.77	-9.21	8.15
301	-4.43	2.98	-7.33	4.98	-9.52	5.85	-10.15	5.32
401	-4.80	2.99	-7.95	4.96	-10.13	4.85	-10.72	4.56

Table 10: $log(l_2 - errors)$ and convergence rates using odd-order upwind SBP operators, for the two-block Euler vortex problem. $\epsilon = 5$. Vortex initiated at $x = 0$ and integrated to $t = 20$, when the vortex has passed the interface.

m	$\log l^2{}_{(2nd)}$	q	$\log l^2{}_{(4th)}$	q	$\log l^2{}_{(6th)}$	q	$\log l^2{}_{(8th)}$	q
51	-2.03	0.00	-3.29	0.00	-3.44	0.00	-3.69	0.00
101	-2.63	1.97	-4.31	3.39	-4.61	3.90	-5.34	5.47
201	-3.23	2.00	-5.26	3.15	-5.80	3.95	-6.85	5.04
301	-3.58	2.00	-5.80	3.06	-6.50	3.97	-7.74	5.00
401	-3.83	2.00	-6.17	3.03	-6.99	3.98	-8.36	4.99

Table 11: $log(l_2 - errors)$ and convergence rates using different traditional operators, for the two-block Euler vortex problem. $\epsilon = 5$. Vortex initiated at $x = 0$ and integrated to $t = 20$, when the vortex has passed the interface.

7 Conclusions

The main focus has been to construct novel diagonal-norm upwind SBP operators with built in artificial dissipation when combined with flux-splitting techniques for hyperbolic systems. This is achieved by allowing non-central difference stencils and introducing a modified SBP definition. The boundary and interface conditions are treated with the SAT technique. The novel upwind SBP operators lead to highly robust and accurate discretizations of hyperbolic problems, corroborated through numerical computations of both linear and nonlinear problems. Numerical computations show that the diagonal-norm upwind SBP operators are superior to the corresponding traditional diagonal-norm SBP operators. For linear first and second order wave equations higher than expected order of convergence is obtained. In a coming study the efficiency of using the new upwind SBP operators in a more complex 3-D setting, with focus on second order hyperbolic systems and hyperbolic-parabolic systems will be analyzed.

APPENDIX

I Diagonal-norm SBP operators

Below the upwind SBP operators, from order 2 up to order 9 are presented. The SBP operators are defined by the coefficients in Q_+ and the norm H. Q_- is given by the relation $Q_- = -Q_+^T$, and it is thus enough to present the coefficients in Q_+ and H. The structure of Q_+ is given by the Ansatz:

$$\begin{bmatrix}
q_{1,1} & q_{1,2} & \cdots & q_{1,s} & & & & & & & & \\
q_{2,1} & \ddots & & q_{2,s} & & & & & & & & \\
\vdots & & & \vdots & q_{\frac{s}{2}+1} & & & & & & & \\
\vdots & & & \vdots & \vdots & & & & & & & \\
q_{s,1} & q_{s,2} & \cdots & q_{s,s} & q_1 & \ddots & \ddots & & & & & \\
 & & q_{n-\frac{s}{2}} & \cdots & q_0 & q_1 & \cdots & q_{\frac{s}{2}+1} & & & & \\
 & & & \ddots & & \ddots & & & \ddots & & & \\
 & & & & q_{n-\frac{s}{2}} & \cdots & q_0 & q_1 & \cdots & q_{\frac{s}{2}+1} & & \\
 & & & & & \ddots & & \ddots & q_{s,s} & q_{s-1,s} & \cdots & q_{1,s} \\
 & & & & & & \ddots & & q_{s,s-1} & \ddots & & q_{1,s-1} \\
 & & & & & & & q_{n-\frac{s}{2}} & \vdots & & & \vdots \\
 & & & & & & & & \vdots & & & \vdots \\
 & & & & & & & & q_{s,1} & \cdots & & q_{1,1}
\end{bmatrix}$$

and $H = h \cdot diag(h_1, \ldots, h_s, 1 \ldots, 1, h_s, \ldots, h_1)$. Let p denote the internal order of accuracy. In the present study $p = 2, 4, 6, 8$ (even order cases) or $p = 3, 5, 7, 9$ (odd order cases). For the odd order cases let $s = p - 1$ and $n = 2$ in the above matrix structure, and for the even order cases let $s = p$ and $n = 1$.

I.1 Second order case

Below, the operators H, Q_+ (and Q_-) for the 2nd order case are presented.

The internal scheme is defined by

$$q_0 = -\tfrac{3}{2} \quad q_1 = 2 \quad q_2 = -\tfrac{1}{2}$$

The coefficients in the norm are given by

$$h_1 = \tfrac{1}{4} \quad h_2 = \tfrac{5}{4}$$

The coefficients in Q_+ are given by

$$q_{1,1} = -\tfrac{1}{4} \quad q_{1,2} = \tfrac{5}{4} \quad q_{2,1} = -\tfrac{1}{4} \quad q_{2,2} = -\tfrac{5}{4}$$

I.2 Third order case

Below, the operators H, Q_+ (and Q_-) for the 3rd order case are presented.

The internal scheme is defined by

$$q_{-1} = -\tfrac{1}{3} \quad q_0 = -\tfrac{1}{2} \quad q_1 = 1 \quad q_2 = -\tfrac{1}{6}$$

The coefficients in the norm are given by

$$h_1 = \tfrac{5}{12} \quad h_2 = \tfrac{13}{12}$$

The coefficients in Q_+ are given by

$$q_{1,1} = -\tfrac{1}{12} \quad q_{1,2} = \tfrac{3}{4} \quad q_{2,1} = -\tfrac{5}{12} \quad q_{2,2} = -\tfrac{5}{12}$$

I.3 Fourth order case

Below, the operators H, Q_+ (and Q_-) for the 4th order case are presented.

The internal scheme is defined by

$$q_{-1} = -\tfrac{1}{4} \quad q_0 = -\tfrac{5}{6} \quad q_1 = \tfrac{3}{2} \quad q_2 = -\tfrac{1}{2} \quad q_3 = \tfrac{1}{12}$$

The coefficients in the norm are given by

$$h_1 = \tfrac{49}{144} \quad h_2 = \tfrac{61}{48} \quad h_3 = \tfrac{41}{48} \quad h_4 = \tfrac{149}{144}$$

The coefficients in Q_+ are given by

$$\begin{array}{llll}
q_{1,1} = -\tfrac{1}{48} & q_{1,2} = \tfrac{205}{288} & q_{1,3} = -\tfrac{29}{144} & q_{1,4} = \tfrac{1}{96} \\
q_{2,1} = -\tfrac{169}{288} & q_{2,2} = -\tfrac{11}{48} & q_{2,3} = \tfrac{33}{32} & q_{2,4} = -\tfrac{43}{144} \\
q_{3,1} = \tfrac{11}{144} & q_{3,2} = -\tfrac{13}{32} & q_{3,3} = -\tfrac{29}{48} & q_{3,4} = \tfrac{389}{288} \\
q_{4,1} = \tfrac{1}{32} & q_{4,2} = -\tfrac{11}{144} & q_{4,3} = -\tfrac{65}{288} & q_{4,4} = -\tfrac{13}{16}
\end{array}$$

I.4 Fifth order case

Below, the operators H, Q_+ (and Q_-) for the 5th order case are presented.

The internal scheme is defined by

$$q_{-2} = \tfrac{1}{20} \quad q_{-1} = -\tfrac{1}{2} \quad q_0 = -\tfrac{1}{3} \quad q_1 = 1 \quad q_2 = -\tfrac{1}{4} \quad q_3 = \tfrac{1}{30}$$

The coefficients in the norm are given by

$$h_1 = \tfrac{251}{720} \quad h_2 = \tfrac{299}{240} \quad h_3 = \tfrac{41}{48} \quad h_4 = \tfrac{149}{144}$$

The coefficients in Q_+ are given by

$$\begin{array}{llll}
q_{1,1} = -\frac{1}{120} & q_{1,2} = \frac{941}{1440} & q_{1,3} = -\frac{47}{360} & q_{1,4} = -\frac{7}{480} \\
q_{2,1} = -\frac{869}{1440} & q_{2,2} = -\frac{11}{120} & q_{2,3} = \frac{25}{32} & q_{2,4} = -\frac{43}{360} \\
q_{3,1} = \frac{29}{360} & q_{3,2} = -\frac{17}{32} & q_{3,3} = -\frac{29}{120} & q_{3,4} = \frac{1309}{1440} \\
q_{4,1} = \frac{1}{32} & q_{4,2} = -\frac{11}{360} & q_{4,3} = -\frac{661}{1440} & q_{4,4} = -\frac{13}{40}
\end{array}$$

I.5 Sixth order case

Below, the operators H, Q_+ (and Q_-) for the 6th order case are presented.

The internal scheme is defined by

$$q_{-2} = \tfrac{1}{30} \quad q_{-1} = -\tfrac{2}{5} \quad q_0 = -\tfrac{7}{12} \quad q_1 = \tfrac{4}{3} \quad q_2 = -\tfrac{1}{2} \quad q_3 = \tfrac{2}{15} \quad q_4 = -\tfrac{1}{60}$$

The coefficients in the norm are given by

$$h_1 = \tfrac{13613}{43200} \quad h_2 = \tfrac{12049}{8640} \quad h_3 = \tfrac{535}{864} \quad h_4 = \tfrac{1079}{864} \quad h_5 = \tfrac{7841}{8640} \quad h_6 = \tfrac{43837}{43200}$$

The coefficients in Q_+ are given by

$$\begin{array}{llll}
q_{1,1} = -\frac{265}{128688} & q_{1,2} = \frac{1146190567}{1737288000} & q_{1,3} = -\frac{1596619}{18384000} & q_{1,4} = -\frac{55265831}{579096000} \\
q_{1,5} = \frac{26269819}{3474576000} & q_{1,6} = \frac{2464501}{144774000} & q_{2,1} = -\frac{1116490567}{1737288000} & q_{2,2} = -\frac{8839}{214480} \\
q_{2,3} = \frac{190538869}{347457600} & q_{2,4} = \frac{102705469}{694915200} & q_{2,5} = \frac{413741}{9651600} & q_{2,6} = -\frac{191689861}{3474576000} \\
q_{3,1} = \frac{1096619}{18384000} & q_{3,2} = -\frac{135385429}{347457600} & q_{3,3} = -\frac{61067}{321720} & q_{3,4} = \frac{45137333}{57909600} \\
q_{3,5} = -\frac{253641811}{694915200} & q_{3,6} = \frac{70665929}{579096000} & q_{4,1} = \frac{66965831}{579096000} & q_{4,2} = -\frac{208765789}{694915200} \\
q_{4,3} = -\frac{17623253}{57909600} & q_{4,4} = -\frac{18269}{45960} & q_{4,5} = \frac{410905829}{347457600} & q_{4,6} = -\frac{477953317}{1158192000} \\
q_{5,1} = -\frac{49219819}{3474576000} & q_{5,2} = \frac{293299}{9651600} & q_{5,3} = \frac{26422771}{694915200} & q_{5,4} = -\frac{141938309}{347457600} \\
q_{5,5} = -\frac{346583}{643440} & q_{5,6} = \frac{2217185207}{1737288000} & q_{6,1} = -\frac{2374501}{144774000} & q_{6,2} = \frac{142906261}{3474576000} \\
q_{6,3} = -\frac{3137129}{579096000} & q_{6,4} = -\frac{29884283}{1158192000} & q_{6,5} = -\frac{630168407}{1737288000} & q_{6,6} = -\frac{3559}{6128}
\end{array}$$

I.6 Seventh order case

Below, the operators H, Q_+ (and Q_-) for the 7th order case are presented.

The internal scheme is defined by

$$q_{-3} = \tfrac{1}{105} \quad q_{-2} = \tfrac{1}{10} \quad q_{-1} = -\tfrac{3}{5} \quad q_0 = -\tfrac{1}{4}$$
$$q_1 = 1 \quad q_2 = -\tfrac{3}{10} \quad q_3 = \tfrac{1}{15} \quad q_4 = -\tfrac{1}{40}$$

The coefficients in the norm are given by

$$h_1 = \tfrac{19087}{60480} \quad h_2 = \tfrac{84199}{60480} \quad h_3 = \tfrac{18869}{30240} \quad h_4 = \tfrac{37621}{30240} \quad h_5 = \tfrac{55031}{60480} \quad h_6 = \tfrac{61343}{60480}$$

The coefficients in Q_+ are given by

$$q_{1,1} = -\tfrac{265}{300272} \quad q_{1,2} = \tfrac{1587945773}{2432203200} \quad q_{1,3} = -\tfrac{1926361}{25737600} \quad q_{1,4} = -\tfrac{84398989}{810734400}$$
$$q_{1,5} = \tfrac{48781961}{4864406400} \quad q_{1,6} = \tfrac{3429119}{202683600} \quad q_{2,1} = -\tfrac{1570125773}{2432203200} \quad q_{2,2} = -\tfrac{26517}{1501360}$$
$$q_{2,3} = \tfrac{240029831}{486440640} \quad q_{2,4} = \tfrac{202934303}{972881280} \quad q_{2,5} = \tfrac{118207}{13512240} \quad q_{2,6} = -\tfrac{231357719}{4864406400}$$
$$q_{3,1} = \tfrac{1626361}{25737600} \quad q_{3,2} = -\tfrac{206937767}{486440640} \quad q_{3,3} = -\tfrac{61067}{750680} \quad q_{3,4} = \tfrac{49602727}{81073440}$$
$$q_{3,5} = -\tfrac{43783933}{194576256} \quad q_{3,6} = \tfrac{51815011}{810734400} \quad q_{4,1} = \tfrac{91418989}{810734400} \quad q_{4,2} = -\tfrac{53314099}{194576256}$$
$$q_{4,3} = -\tfrac{33094279}{81073440} \quad q_{4,4} = -\tfrac{18269}{107240} \quad q_{4,5} = \tfrac{440626231}{486440640} \quad q_{4,6} = -\tfrac{365711063}{1621468800}$$
$$q_{5,1} = -\tfrac{62551961}{4864406400} \quad q_{5,2} = \tfrac{799}{35280} \quad q_{5,3} = \tfrac{82588241}{972881280} \quad q_{5,4} = -\tfrac{279245719}{486440640}$$
$$q_{5,5} = -\tfrac{346583}{1501360} \quad q_{5,6} = \tfrac{2312302333}{2432203200} \quad q_{6,1} = -\tfrac{3375119}{202683600} \quad q_{6,2} = \tfrac{202087559}{4864406400}$$
$$q_{6,3} = -\tfrac{11297731}{810734400} \quad q_{6,4} = \tfrac{61008503}{1621468800} \quad q_{6,5} = -\tfrac{1360092253}{2432203200} \quad q_{6,6} = -\tfrac{10677}{42896}$$

I.7 Eighth order case

Below, the operators H, Q_+ (and Q_-) for the 8th order case are presented.

The internal scheme is defined by

$$q_{-3} = -\tfrac{1}{168} \quad q_{-2} = \tfrac{1}{14} \quad q_{-1} = -\tfrac{1}{2} \quad q_0 = -\tfrac{9}{20}$$
$$q_1 = \tfrac{5}{4} \quad q_2 = -\tfrac{1}{2} \quad q_3 = \tfrac{1}{6} \quad q_4 = -\tfrac{1}{28} \quad q_5 = \tfrac{1}{280}$$

The coefficients in the norm are given by

$$h_1 = \tfrac{7489399}{25401600} \quad h_2 = \tfrac{5537831}{3628800} \quad h_3 = \tfrac{103373}{403200} \quad h_4 = \tfrac{261259}{145152}$$
$$h_5 = \tfrac{298231}{725760} \quad h_6 = \tfrac{515917}{403200} \quad h_7 = \tfrac{3349159}{3628800} \quad h_8 = \tfrac{25639991}{25401600}$$

The coefficients in Q_+ are given by

$$q_{1,1} = -\frac{16683}{63018560} \quad q_{1,2} = \frac{29345822969987}{43354248537600} \quad q_{1,3} = -\frac{2734625426591}{40644608004000} \quad q_{1,3} = -\frac{113480208109603}{780376473676800}$$
$$q_{1,5} = -\frac{830250230261}{26012549122560} \quad q_{1,6} = \frac{2500519492033}{32515686403200} \quad q_{1,7} = \frac{2235718279643}{390188236838400} \quad q_{1,8} = -\frac{388481888477}{26543417472000}$$
$$q_{2,1} = -\frac{29227665839987}{43354248537600} \quad q_{2,2} = -\frac{493793}{63018560} \quad q_{2,3} = \frac{8302717120817}{26543417472000} \quad q_{2,4} = \frac{3739408501537}{9290196115200}$$
$$q_{2,5} = \frac{2684481534461}{13935294172800} \quad q_{2,6} = -\frac{4450185662513}{18580392230400} \quad q_{2,7} = -\frac{1221838279381}{37160784460800} \quad q_{2,8} = \frac{90595000956023}{1950941184192000}$$
$$q_{3,1} = \frac{2505689537591}{40644608004000} \quad q_{3,2} = -\frac{7312922392817}{26543417472000} \quad q_{3,3} = -\frac{69332623}{1323389760} \quad q_{3,4} = \frac{10994933811709}{18580392230400}$$
$$q_{3,5} = -\frac{9270952411151}{18580392230400} \quad q_{3,6} = \frac{3191238635141}{20644880256000} \quad q_{3,7} = \frac{4442211176987}{92901961152000} \quad q_{3,8} = -\frac{940661365031}{32515686403200}$$
$$q_{4,1} = \frac{118016946570403}{780376473676800} \quad q_{4,2} = -\frac{4173878828737}{9290196115200} \quad q_{4,3} = -\frac{7990503962509}{18580392230400} \quad q_{4,4} = -\frac{207799621}{1323389760}$$
$$q_{4,5} = \frac{2044021560341}{2477385630720} \quad q_{4,6} = \frac{511197701761}{18580392230400} \quad q_{4,7} = \frac{1237681717213}{13935294172800} \quad q_{4,8} = -\frac{7784834666617}{130062745612800}$$
$$q_{5,1} = \frac{68609076271}{2364777192960} \quad q_{5,2} = -\frac{2235651762161}{13935294172800} \quad q_{5,3} = \frac{6527681584751}{18580392230400} \quad q_{5,4} = -\frac{1115980068821}{2477385630720}$$
$$q_{5,5} = -\frac{55386253}{189055680} \quad q_{5,6} = \frac{3208334350649}{3716078446080} \quad q_{5,7} = -\frac{407569013461}{844563283200} \quad q_{5,8} = \frac{136474842626653}{780376473676800}$$
$$q_{6,1} = -\frac{2487637785013}{32515686403200} \quad q_{6,2} = \frac{4244231077313}{18580392230400} \quad q_{6,3} = -\frac{1550378843141}{20644880256000} \quad q_{6,4} = -\frac{5726967564961}{18580392230400}$$
$$q_{6,5} = -\frac{1017898941929}{3716078446080} \quad q_{6,6} = -\frac{526653889}{1323389760} \quad q_{6,7} = \frac{45241297077547}{37160784460800} \quad q_{6,8} = -\frac{2279608411897}{5080576000500}$$
$$q_{7,1} = -\frac{2164019088443}{390188236838400} \quad q_{7,2} = \frac{1263196075861}{37160784460800} \quad q_{7,3} = -\frac{6600697610987}{92901961152000} \quad q_{7,4} = \frac{556610591687}{13935294172800}$$
$$q_{7,5} = \frac{926842346471}{9290196115200} \quad q_{7,6} = -\frac{18757693936747}{37160784460800} \quad q_{7,7} = -\frac{584765899}{1323389760} \quad q_{7,8} = \frac{204646287449}{168431424000}$$
$$q_{8,1} = \frac{387091928477}{26543417472000} \quad q_{8,2} = -\frac{90231551688023}{1950941184192000} \quad q_{8,3} = \frac{1032404418251}{32515686403200} \quad q_{8,4} = \frac{3502353445417}{130062745612800}$$
$$q_{8,5} = -\frac{15385068876253}{780376473676800} \quad q_{8,6} = \frac{262499068919}{10161152001000} \quad q_{8,7} = -\frac{867004691939}{1852745664000} \quad q_{8,8} = -\frac{85017967}{189055680}$$

I.8 Ninth order case

Below, the operators H, Q_+ (and Q_-) for the 9th order case are presented.

The internal scheme is defined by

$$q_{-4} = \frac{1}{504} \quad q_{-3} = -\frac{1}{42} \quad q_{-2} = \frac{1}{7} \quad q_{-1} = -\frac{2}{3} \quad q_0 = -\frac{1}{5}$$
$$q_1 = 1 \quad q_2 = -\frac{1}{3} \quad q_3 = \frac{2}{21} \quad q_4 = -\frac{1}{56} \quad q_5 = \frac{1}{630}$$

The coefficients in the norm are given by

$$h_1 = \frac{1070017}{3628800} \quad h_2 = \frac{5537111}{3628800} \quad h_3 = \frac{103613}{403200} \quad h_4 = \frac{261115}{145152}$$
$$h_5 = \frac{298951}{725760} \quad h_6 = \frac{515677}{403200} \quad h_7 = \frac{3349879}{3628800} \quad h_8 = \frac{3662753}{3628800}$$

The coefficients in Q_+ are given by

$$
\begin{array}{llll}
q_{1,1} = -\frac{5561}{47263920} & q_{1,2} = \frac{4186300102421}{6193464076800} & q_{1,3} = -\frac{377895002003}{5806372572000} & q_{1,4} = -\frac{16485548951749}{111482353382400} \\
q_{1,5} = -\frac{113245973003}{3716078446080} & q_{1,6} = \frac{355360297339}{4645098057600} & q_{1,7} = \frac{321012170669}{55741176691200} & q_{1,8} = -\frac{388397049437}{26543417472000} \\
q_{2,1} = -\frac{4178798062421}{6193464076800} & q_{2,2} = -\frac{493793}{141791760} & q_{2,3} = \frac{725405227507}{2413037952000} & q_{2,4} = \frac{3904159533697}{9290196115200} \\
q_{2,5} = \frac{2483046570341}{13935294172800} & q_{2,6} = -\frac{4336328670953}{18580392230400} & q_{2,7} = -\frac{1258688487061}{37160784460800} & q_{2,8} = \frac{12931584852209}{278705883456000} \\
q_{3,1} = \frac{363359390003}{5806372572000} & q_{3,2} = -\frac{7539548734577}{26543417472000} & q_{3,3} = -\frac{69332623}{2977626960} & q_{3,4} = \frac{9994352248429}{18580392230400} \\
q_{3,5} = -\frac{8195655811631}{18580392230400} & q_{3,6} = \frac{7361486640463}{61934640768000} & q_{3,7} = \frac{5539855071347}{92901961152000} & q_{3,8} = -\frac{12898722943}{422281641600} \\
q_{4,1} = \frac{16773595838149}{111482353382400} & q_{4,2} = -\frac{372477950627}{844563283200} & q_{4,3} = -\frac{8659050093229}{18580392230400} & q_{4,4} = -\frac{207799621}{2977626960} \\
q_{4,5} = \frac{1734921317461}{2477385630720} & q_{4,6} = \frac{2530020015841}{18580392230400} & q_{4,7} = \frac{441856623253}{13935294172800} & q_{4,8} = -\frac{115132773073}{2654341747200} \\
q_{5,1} = \frac{108449122763}{3716078446080} & q_{5,2} = -\frac{2283566671541}{13935294172800} & q_{5,3} = \frac{6976424333231}{18580392230400} & q_{5,4} = -\frac{440819477447}{825795210240} \\
q_{5,5} = -\frac{55386253}{425375280} & q_{5,6} = \frac{2479572560009}{3716078446080} & q_{5,7} = -\frac{40258468963}{120651897600} & q_{5,8} = \frac{11808221047099}{111482353382400} \\
q_{6,1} = -\frac{32231128289}{422281641600} & q_{6,2} = \frac{4244793299753}{18580392230400} & q_{6,3} = -\frac{5173673584463}{61934640768000} & q_{6,4} = -\frac{4848139955041}{18580392230400} \\
q_{6,5} = -\frac{1506045711689}{3716078446080} & q_{6,6} = -\frac{526653889}{2977626960} & q_{6,7} = \frac{36411368691307}{37160784460800} & q_{6,8} = -\frac{825434105779}{2903186286000} \\
q_{7,1} = -\frac{316459841069}{55741176691200} & q_{7,2} = \frac{1277069729941}{37160784460800} & q_{7,3} = -\frac{6499182375347}{92901961152000} & q_{7,4} = \frac{355606625147}{13935294172800} \\
q_{7,5} = \frac{1519272420551}{9290196115200} & q_{7,6} = -\frac{2240079855137}{3378253132800} & q_{7,7} = -\frac{584765899}{2977626960} & q_{7,8} = \frac{2301241355533}{2382101568000} \\
q_{8,1} = \frac{387779289437}{26543417472000} & q_{8,2} = -\frac{12908508708209}{278705883456000} & q_{8,3} = \frac{147710908133}{4645098057600} & q_{8,4} = \frac{534025841911}{18580392230400} \\
q_{8,5} = -\frac{4119981443899}{111482353382400} & q_{8,6} = \frac{279819152779}{2903186286000} & q_{8,7} = -\frac{1510324515533}{2382101568000} & q_{8,8} = -\frac{85017967}{425375280}
\end{array}
$$

References

[1] Saul Abarbanel and Adi Ditkowski. Asymptotically stable fourth-order accurate schemes for the diffusion equation on complex shapes. *Journal of Computational Physics*, 133(2):279 – 288, 1997.

[2] M. Almquist, K. Mattsson, and T. Edvinsson. High-fidelity numerical solution of the time-dependent Dirac equation. *J. Comput. Phys.*, 262:86–103, 2014.

[3] A. Bayliss, K. E. Jordan, B. J. Lemesurier, and E. Turkel. A fourth order accurate finite difference scheme for the computation of elastic waves. *Bull. Seismol. Soc. Amer.*, 76(4):1115–1132, 1986.

[4] M. H. Carpenter, D. Gottlieb, and S. Abarbanel. Time-stable boundary conditions for finite-difference schemes solving hyperbolic systems: Methodology and application to high-order compact schemes. *J. Comput. Phys.*, 111(2):220–236, 1994.

[5] David C. Del Rey Fernández, Pieter D. Boom, and David W. Zingg. A generalized framework for nodal first derivative summation-by-parts operators. *J. Comput. Phys.*, 266:214–239, June 2014.

[6] Leonid Dovgilovich and Ivan Sofronov. High-accuracy finite-difference schemes for solving elastodynamic problems in curvilinear coordinates within multiblock approach. *Appl. Numer. Math.*, 93(C):176–194, July 2015.

[7] Kenneth Duru and Kristoffer Virta. Stable and high order accurate difference methods for the elastic wave equation in discontinuous media. *Journal of Computational Physics*, 279:37 – 62, 2014.

[8] B.A. Erickson and J. Nordström. High order accurate adaptive schemes for long time, highly intermittent geophysics problems. *Journal of Computational and Applied Mathematics*, 271:328 – 338, 2014.

[9] B. Gustafsson, H.-O. Kreiss, and J. Oliger. *Time dependent problems and difference methods*. John Wiley & Sons, Inc., 1995.

[10] Jan S. Hesthaven. A stable penalty method for the compressible Navier-Stokes equations: III. multidimensional domain decomposition schemes. *SIAM Journal on Scientific Computing*, 20:62–93, 1998.

[11] J.E. Hicken. Output error estimation for summation-by-parts finite-difference schemes. *Journal of Computational Physics*, 231(9):3828 – 3848, 2012.

[12] H.-O. Kreiss and G. Scherer. Finite element and finite difference methods for hyperbolic partial differential equations. *Mathematical Aspects of Finite Elements in Partial Differential Equations., Academic Press, Inc.*, 1974.

[13] Heinz-Otto Kreiss and Joseph Oliger. Comparison of accurate methods for the integration of hyperbolic equations. *Tellus XXIV*, 3, 1972.

[14] S. K. Lele. Compact finite difference schemes with spectral-like resolution. *J. Comput. Phys.*, 103:16–42, 1992.

[15] K. Mattsson and M. Almquist. A solution to the stability issues with block norm summation by parts operators. *J. Comput. Phys.*, 253:418–442, 2013.

[16] K. Mattsson, M. Almquist, and M. H. Carpenter. Optimal diagonal-norm SBP operators. *J. Comput. Phys.*, 264:91–111, 2014.

[17] K. Mattsson, F. Ham, and G. Iaccarino. Stable and accurate wave propagation in discontinuous media. *J. Comput. Phys.*, 227:8753–8767, 2008.

[18] K. Mattsson and J. Nordström. Summation by parts operators for finite difference approximations of second derivatives. *J. Comput. Phys.*, 199(2):503–540, 2004.

[19] K. Mattsson and J. Nordström. High order finite difference methods for wave propagation in discontinuous media. *J. Comput. Phys.*, 220:249–269, 2006.

[20] K. Mattsson, M. Svärd, M.H. Carpenter, and J. Nordström. High-order accurate computations for unsteady aerodynamics. *Computers & Fluids*, 36:636–649, 2006.

[21] K. Mattsson, M. Svärd, and M. Shoeybi. Stable and accurate schemes for the compressible navier-stokes equations. *J. Comput. Phys.*, 227(4):2293–2316, 2008.

[22] Ken Mattsson. Summation by parts operators for finite difference approximations of second-derivatives with variable coefficients. *Journal of Scientific Computing*, 51:650–682, 2012.

[23] Ken Mattsson. Diagonal-norm summation by parts operators for finite difference approximations of third and fourth derivatives. *J. Comput. Phys.*, 274(0):432 – 454, 2014.

[24] Ken Mattsson and Jonatan Werpers. High-fidelity numerical simulation of solitons in the nerve axon. *Journal of Computational Physics*, 305:793 – 816, 2016.

[25] Anna Nissen, Katharina Kormann, Magnus Grandin, and Kristoffer Virta. Stable difference methods for block-oriented adaptive grids. *Journal of Scientific Computing*, pages 1–26, 2014.

[26] J. Nordström and M. Svärd. Well Posed Boundary Conditions for the Navier-Stokes Equations. *SIAM Journal on Numerical Analysis*, 43(3):1231–1255, September 2005.

[27] P. Olsson. Summation by parts, projections, and stability I. *Math. Comp.*, 64:1035, 1995.

[28] P. Olsson. Summation by parts, projections, and stability II. *Math. Comp.*, 64:1473, 1995.

[29] N. Anders Petersson, Ossian O'Reilly, Björn Sjögreen, and Samuel Bydlon. Discretizing singular point sources in hyperbolic wave propagation problems. *Journal of Computational Physics*, pages –, 2016.

[30] S. De Rango and D. W. Zingg. A high-order spatial discretization for turbulent aerodynamic computations. *AIAA J.*, 39(7):1296–1304, 2001.

[31] B. Strand. Summation by parts for finite difference approximations for d/dx. *J. Comput. Physics*, 110:47–67, 1994.

[32] John C. Strikwerda. High-order-accurate schemes for incompressible viscous flow. *International Journal for Numerical Methods in Fluids*, 24:715–734, 1997.

[33] M. Svärd. On coordinate transformation for summation-by-parts operators. *Journal of Scientific Computing*, 20(1), 2004.

[34] M. Svärd, M. H. Carpenter, and J. Nordström. A stable high-order finite difference scheme for the compressible Navier–Stokes equations, far-field boundary conditions. *J. Comput. Physics*, 225:1020–1038, February 2008.

[35] M. Svärd, M. H. Carpenter, and J. Nordström. A stable high-order finite difference scheme for the compressible Navier–Stokes equations, no-slip wall boundary conditions. *J. Comput. Physics*, 227:4805–4824, May 2008.

[36] M. Svärd, K. Mattsson, and J. Nordström. Steady-state computations using summation-by-parts operators. *Journal of Scientific Computing*, 24(1):79–95, July 2005.

[37] M. Svärd and J. Nordström. On the order of accuracy for difference approximations of initial-boundary value problems. *J. Comput. Physics*, 218:333–352, October 2006.

[38] Kristoffer Virta and Ken Mattsson. Acoustic wave propagation in complicated geometries and heterogeneous media. *Journal of Scientific Computing*, 61(1):90–118, 2014.